CHEMISTRY OF MATERIALS

pubs.acs.org/cm

Article

Minute and Large-Scale Synthesis of Covalent-Organic Frameworks in Water at Room Temperature by a Two-Step Dissolution−Precipitation Method

Liecheng Guo, Qing Yun Zhang, Zhiwu Yu,* Rajamani Krishna, and Feng Luo*

Cite This: *Chem. Mater.* 2023, 35, 5648−5656

Read Online

ACCESS | Metrics & More | Article Recommendations | Supporting Information

ABSTRACT: Low-cost, green, large-scale, room-temperature, and fast synthesis of covalent organic frameworks (COFs) represents a highly desirable issue, due to both scientific and industrial interests, but remains a big challenge. The disadvantage of the established solvothermal method for COFs is now seriously restricting their practical industrial applications. We report herein aqueous synthesis of ketoenamine- and imine-linked COFs through a two-step dissolution−precipitation (DP) strategy. Impressively, using this DP method, we can prepare five ketoenamine-linked COFs and two imine-linked COFs in an ideal synthetic process with room temperature, 5 min reaction time, and large-scale products for one batch reaction, in the absence of acetic acid. These COFs show impressively high crystallinity and porosity and potential application in iodine and uranyl capture. This ideal synthetic route will pave a powerful methodology for making functional COFs with the value of practical industrial applications.

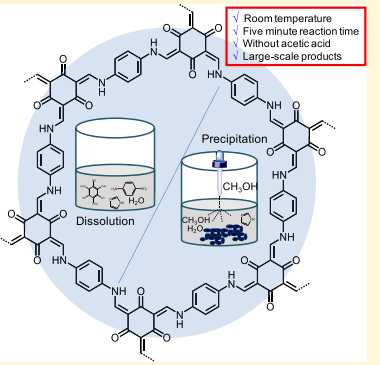

1. INTRODUCTION

Crystalline covalent organic frameworks (COFs) represent a newly developed porous platform, which are constructed from high bond-energy covalent bonds and light elements, thus affording unique physical and chemical properties and a broad outstanding application in catalysis, adsorption, separation, chemosensing, drug delivery, energy storage, radionuclide capture, and so on.[1−17] However, there still remains a serious concern about the synthesis of COFs because, typically, previous COFs have been mainly prepared through the solvothermal method under sealed degassed tubes at high temperatures (120−200 °C), long reaction times (3−7 days), and toxic organic solvents (like mesitylene, 1,2-dioxane, and o-dichlorobenzene) with a low output for one batch reaction (less than 100 mg).[1−17] Such rigorous recipes (Scheme 1) in the synthesis of COFs seriously restrict their practical industrial applications. Therefore, there is an urgent need for a safer, cleaner, simpler, and more economical route for COF synthesis.

Methods of substituting solvothermal synthesis include, but not limited to, microwave and catalytic synthesis,[18,19] as well as electron beam irradiation,[20] which can largely reduce the reaction temperature to room temperature and reaction time to 1−2 h. However, they still required toxic organic solvents and metal catalysts. To avoid the use of toxic organic solvents, solid-state synthesis represents a desirable route. However, a high reaction temperature (200 °C) and long reaction time (1−7 days) were often required.[21,22] For example, the melt polymerization method was exploited for the synthesis of covalent triazine frameworks and olefin-linked COFs, respectively, which called for a high-reaction temperature (200 °C) and long reaction time (7 days).[23,24] Moreover, Fang et al. recently reported the preparation of 3D COFs with ionic liquids as solvents at room temperature within 3 min,[25] but this is just amenable to small-scale discovery chemistry (low output of less than 50 mg for one batch reaction).

Synthesis of COFs in water represents another attractive avenue for pursuit. However, this would be majorly blocked from the low solubility of organic monomer in water.[26,27] As a result, there was only few reports of ketoenamine-based COFs that could be prepared through the hydrothermal method.[26,27] But, it still requires some unfavorable conditions, such as relatively high reaction temperatures (>120 °C) and long reaction time (0.5−3 days). Furthermore, Zamora developed the synthesis of imine-bridged COFs in water under relatively mild conditions (80 °C and 5 h).[28] In order to increase the solubility of organic monomers in water, they just used very low concentrations for starting monomers, which would seriously restrict its practical industrial applications. At the same time, this method also required a suitable pH value adjusted by acetic acid and powerful microwave assistance. Impressively, a recent report from Cooper and co-workers

Received: May 18, 2023
Revised: June 22, 2023
Published: July 6, 2023

Scheme 1. Comparison of COF Synthesis between Established Methods and Our Route

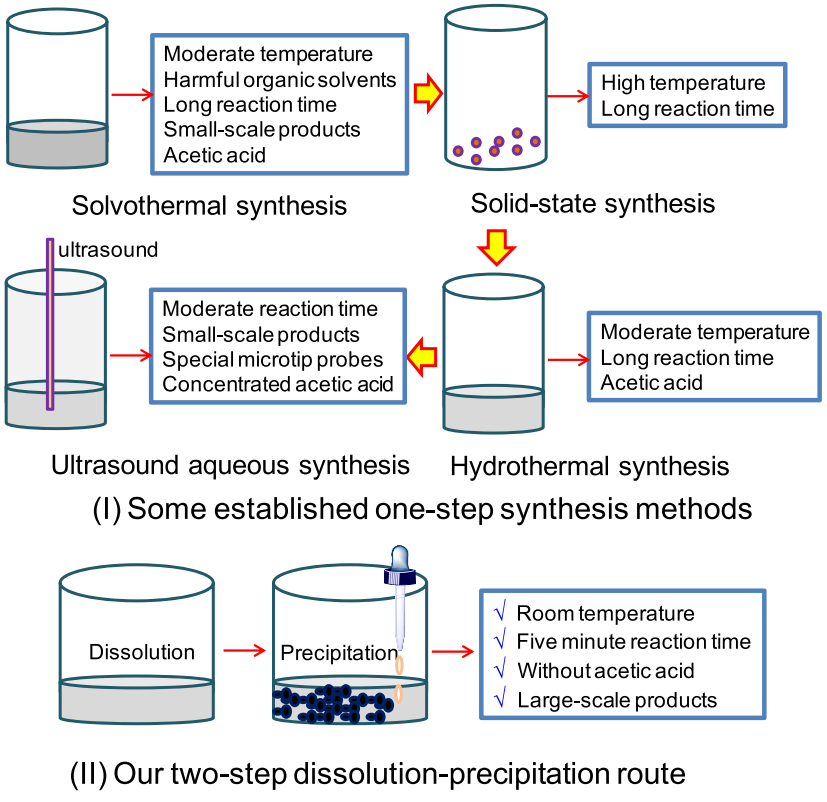

advocates the aqueous synthesis of imine-linked COFs at room temperature and a short reaction time of 1 h, but their synthesis demanded high concentrations of acetic acid (6−9 M) as the solvent and powerful ultrasound assistance with microtip probes (550 W power output).[29] In addition, the use of microtip probes inevitably led to low output (<100 mg) for one batch reaction.

Despite the above-mentioned developments, there still lacks a large-scale synthesis route, which can be operated at room temperature and short reaction time (minute level) without green solvents (or solvent-free). Toward this end, we present a two-step dissolution−precipitation (DP) strategy for large-scale synthesis of ketoenamine- and imine-linked COFs in water at room temperature and minute reaction time without the use of acetic acid (Scheme 1). Although the addition of imidazole and methanol was the key factor in our synthesis strategy, however, both imidazole and methanol are commercially available products with extremely low prices of about 10 and 1 $/1 kg, respectively. Thus, the use of imidazole and methanol herein does not increase synthesis cost.

2. EXPERIMENTAL SECTION

2.1. Synthesis of dpCOF-1. A mixture of A1 (49 mg, 0.45 mmol), T (63 mg, 0.3 mmol), and imidazole (200 mg, 3 mmol) was mixed in a beaker (10 mL) in 10 mL water, then it was stirred for 5 min, and a clear solution was observed. Adding 50 mL CH_3OH into the above solution will immediately regenerate a large amount of precipitation. The solid was collected and washed in-turn with DMF, water, and methanol. The powder samples were dried at 80 °C under vacuum overnight to give dpCOF in ∼96% yield.

2.2. Large-Scale Synthesis of dpCOF-1. A mixture of A1 (660 mg, 6 mmol), T (840 mg, 4 mmol), and imidazole (2 g, 3 mol) was mixed in a beaker (1 L) in 100 mL water, then it was stirred for 5 min, and a clear solution was observed. Adding 500 mL CH_3OH into the above solution will immediately regenerate a large amount of precipitation. The solid was collected and washed in-turn with DMF, water, and methanol. The powder samples were dried at 80 °C under vacuum overnight to give dpCOF in ∼94% yield.

2.3. Large-Scale Synthesis of dpCOF-2. A mixture of A2 (830 mg, 4.5 mmol), T (630 mg, 3 mmol), and imidazole (2 g, 3 mol) was mixed in a beaker (1 L) in 100 mL water, then it was stirred for 5 min, and a clear solution was observed. Adding 500 mL CH_3OH into the above solution will immediately regenerate a large amount of precipitation. The solid was collected and washed in-turn with DMF, water, and methanol. The powder samples were dried at 80 °C under vacuum overnight to give dpCOF in ∼92% yield.

2.4. Large-Scale Synthesis of dpCOF-3. A mixture of A3 (318 mg, 3 mmol), T (630 mg, 3 mmol), and imidazole (2 g, 3 mol) was mixed in a beaker (1 L) in 100 mL water, then it was stirred for 5 min, and a clear solution was observed. Adding 500 mL CH_3OH into the above solution will immediately regenerate a large amount of precipitation. The solid was collected and washed in-turn with DMF, water, and methanol. The powder samples were dried at 80 °C under vacuum overnight to give dpCOF in ∼93% yield.

2.5. Large-Scale Synthesis of dpCOF-4. A mixture of A4 (570 mg, 3 mmol), T (630 mg, 3 mmol), and imidazole (1.5 g, 2.2 mol) was mixed in a beaker (1 L) in 100 mL water, then it was stirred for 5 min, and a clear solution was observed. Adding 500 mL CH_3OH into the above solution will immediately regenerate a large amount of precipitation. The solid was collected and washed in-turn with DMF, water, and methanol. The powder samples were dried at 80 °C under vacuum overnight to give dpCOF in ∼82% yield.

2.6. Large-Scale Synthesis of dpCOF-5. A mixture of A5 (1 g, 3 mmol), T (630 mg, 3 mmol), and imidazole (1.5 g, 2.2 mol) was mixed in a beaker (1 L) in 100 mL water, then it was stirred for 5 min, and a clear solution was observed. Adding 500 mL CH_3OH into the above solution will immediately regenerate a large amount of precipitation. The solid was collected and washed in-turn with DMF, water, and methanol. The powder samples was dried at 80 °C under vacuum overnight to give the dpCOF in ∼79% yield.

https://doi.org/10.1021/acs.chemmater.3c01220
Chem. Mater. 2023, 35, 5648−5656

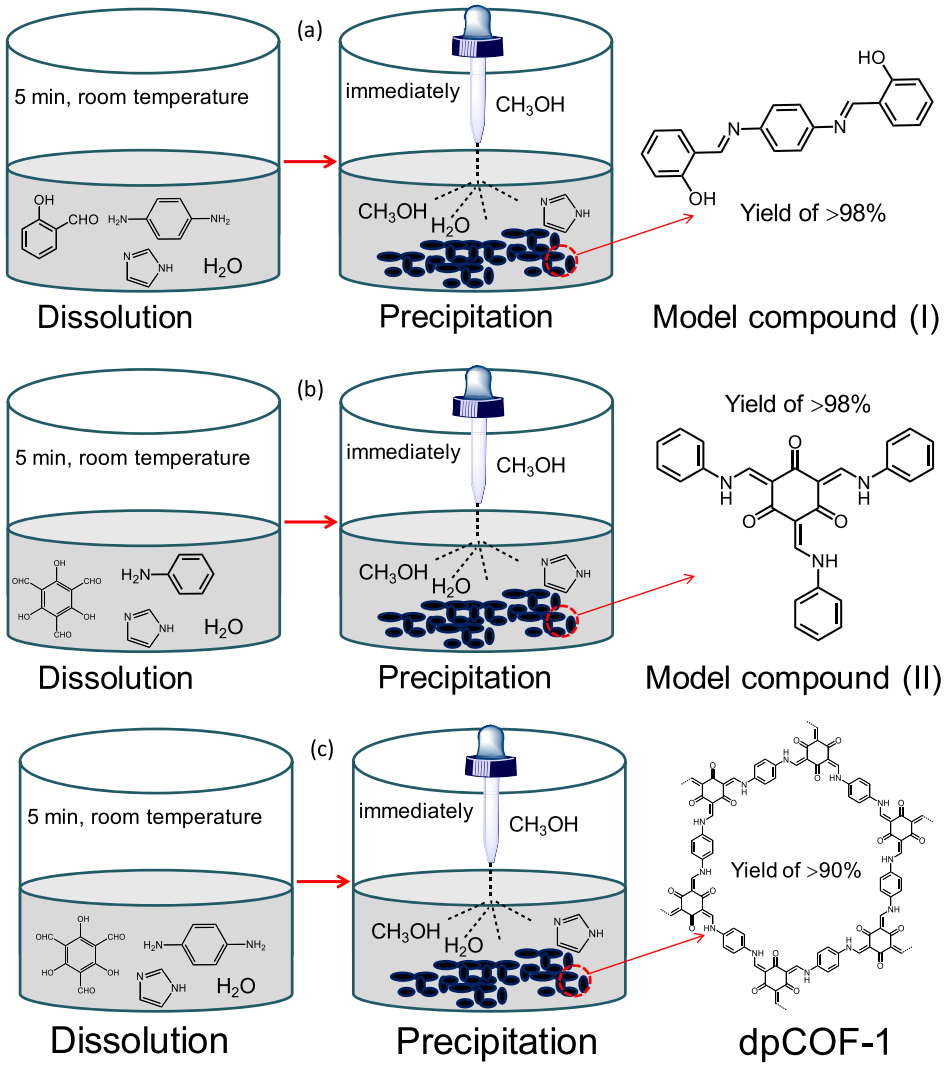

Figure 1. View of the synthesis of model compounds (a,b) and dpCOF-1(c) through our two-step DP method.

2.7. Large-Scale Synthesis of dpCOF-6. A mixture of A1 (660 mg, 6 mmol), Y (648 mg, 4 mmol), and imidazole (2 g, 3 mol) was mixed in a beaker (1 L) in 100 mL water, then it was stirred for 5 min, and a clear solution was observed. Adding 500 mL CH_3OH into the above solution will immediately regenerate a large amount of precipitation. The solid was collected and washed in-turn with DMF, water, and methanol. The powder samples were dried at 80 °C under vacuum overnight to give dpCOF in ~97% yield.

2.8. Large-Scale Synthesis of dpCOF-7. A mixture of A2 (830 mg, 4.5 mmol), Y (648 mg, 4 mmol), and imidazole (2 g, 3 mol) was mixed in a beaker (1 L) in 100 mL water, then it was stirred for 5 min, and a clear solution was observed. Adding 500 mL CH_3OH into the above solution will immediately regenerate a large amount of precipitation. The solid was collected and washed in-turn with DMF, water, and methanol. The powder samples were dried at 80 °C under vacuum overnight to give dpCOF in ~95% yield.

3. RESULTS AND DISCUSSION

3.1. Synthesis and Structure of Model Compounds. As discussed above, the stumbling block of aqueous phase synthesis is the low solubility of organic monomers in water. To solve this problem, we found that the presence of imidazole could largely promote the solubility of organic monomers in water. First, we investigated the model reaction between 2-hydroxybenzaldehyde (H) and benzene-1,4-diamine (A1) through aqueous synthesis (Figure 1a). It is found that stirring aqueous solution containing H, A1, and imidazole in water at room temperature for 5 min will result in the completely dissolved solution, and next adding CH_3OH into this solution will immediately generate the model compound. The yield was >98%. By contrast, a similar synthesis process with the absence of imidazole still gave the completely dissolved solution, but just little product with a low yield of 20%. The results imply that the presence of imidazole could not only promote the Schiff base reaction but also restrain its reversible nature. The model compound (I) was well resolved by ^{1}H nuclear magnetic resonance (NMR) (Figure S1) and single-crystal X-ray diffraction. As shown in Figure S2, it is found that H and A1 are covalently connected through the formation of two imine bonds (C═N) with a bond length of 1.284(4) Å in a trans-configuration. A co-planar structure is found for this model molecule. Intramolecular O−H···N hydrogen bonds (2.607(4) Å) are observed. Significant $\pi-\pi$ [centroid-to-centroid distances of 3.326(5) and 3.269(5) Å] interactions between the C═N bond and phenyl provide the major contribution to stabilize the stacking architecture (Figure S3). We further carried out the model reaction between 2,4,6-trihydroxybenzene-1,3,5-tricarbaldehyde (T) and aniline through aqueous synthesis (Figure 1b). Impressively, the

https://doi.org/10.1021/acs.chemmater.3c01220
Chem. Mater. 2023, 35, 5648−5656

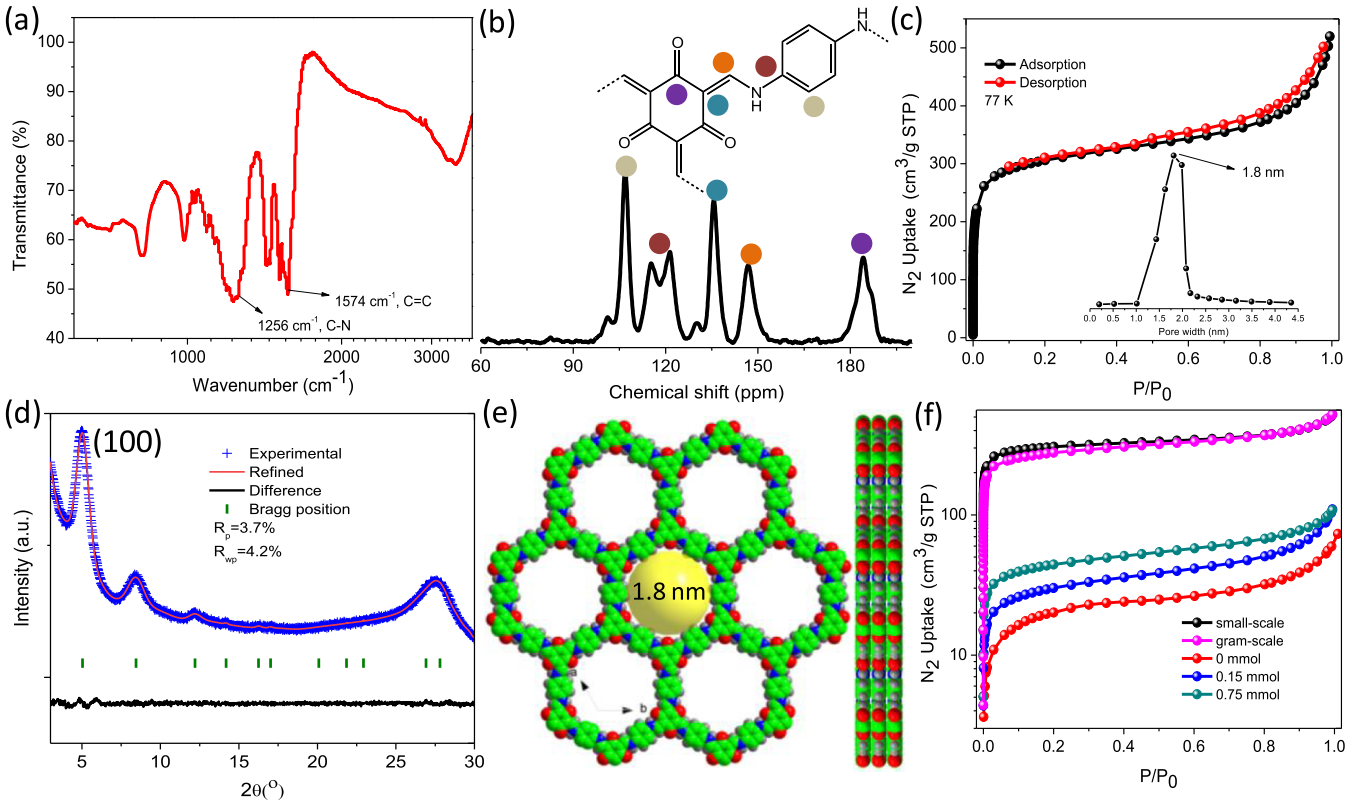

Figure 2. (a) IR spectra of dpCOF-1. (b) Solid-state ^{13}C NMR spectra of dpCOF-1. (c) N_2 adsorption/desorption isotherms of dpCOF-1 at 77 K with the inset of aperture distribution. (d) Experimental (blue dot) and simulated (red line) PXRD patterns of dpCOF-1. (e) Structure of dpCOF-1 with AA eclipsed stacking models. (f) Comparison of porosity of dpCOF-1 synthesized under various conditions.

absence of imidazole could result in an undissolved solution because of the low solubility of T monomers, while the presence of imidazole gave a completely dissolved solution. This strongly suggests the dissolution effect from imidazole. Similarly, the model compound (II) can be immediately generated with a high yield of >98%. Moreover, its structure was further determined by ^1H NMR (Figure S4), where β-ketoenamine-linked structures were confirmed.

3.2. Synthesis and Structure of dpCOF-1. The success in aqueous synthesis of model compounds by means of the DP method through a Schiff base reaction prompted us to extend it for synthesis of crystalline COFs by means of Schiff base reaction. Accordingly, we initially selected the well-known ketoenamine-linked COF of TpPa-1 as a representative investigation.[21,22] In order to distinguish with previously synthesized TpPa-1 using other methods, our prepared product was named dpCOF-1. Typically, dpCOF-1 was obtained as follows, first, stirring the aqueous solution containing an organic monomer of A1 (0.45 mmol) and 2,4,6-trihydroxybenzene-1,3,5-tricarbaldehyde (T, 0.3 mmol) in the presence of imidazole (3 mmol) for 5 min at room temperature (Figure 1c), leading to a completely dissolved solution (Figure S5), and then adding CH_3OH into this solution, immediately forming a target product (Figure S5). Fourier transform infrared (IR) spectra of dpCOF-1 was in agreement with those reported previously, where strong peaks at 1256 cm^{-1} (C−N) and 1574 cm^{-1} (C═C) were observed (Figure 2a),[6,7] implying the formation of β-ketoenamine-linked structure. This was further confirmed by solid-state ^{13}C NMR spectra, showing a characteristic peak of carbonyl carbon (C═O) at 184 ppm (Figure 2b). Other assignments in detail are shown in Figure 2b. The scanning electron microscopy (SEM) image revealed a particulate morphology with the uniform distribution of C, O, and N elements in the energy-dispersive spectroscopy (EDS) (Figure S6). The permanent porosity was confirmed by N_2 adsorption at 77 K, giving a Brunauer−Emmett−Teller (BET) surface area of 954 m^2/g, pore volume of 0.8 cm^3/g, and aperture of 1.8 nm (Figure 2c). It is noteworthy that there is almost 1.8-fold enhancement in the BET surface area, relative to the previously reported solvothermal counterpart.[21] The structure of dpCOF-1 was revealed by powder X-ray diffraction (PXRD) plus Pawley refinement of PXRD data (Figure 2d). High crystallinity was observed, as evidenced by the relatively high-intensity (100) peak reflect. The structural data revealed a hexagonal crystal system with a $P6/m$ space group, cell parameters of $a = b =$ 22.9139 Å and c = 3.4273 Å, and AA eclipsed stacking models (Figure 2e). Moreover, the experimental pore size (1.8 nm) is consistent with the estimated value from simulated structural data (1.8 nm).

3.3. Imidazole Effect on dpCOF-1. It was found that the consumed amount of imidazole has a significant effect on the resultant samples with various crystallinity (Figure S7) and porosity (Figure 2f). For example, the as-synthesized samples in the absence of imidazole yielded no crystallinity and small N_2 adsorption at 77 K, suggesting negligible porosity. Poor crystallinity and negligible porosity were also observed when using 0.15 mmol imidazole. By contrast, crystallinity and porosity slightly increased along with increasing input amount of imidazole, such as 0.75 mmol. Only the input amount reached 2 mmol, then we can obtain highly crystalline COFs of dpCOF-1. Moreover, the solubility of organic monomers in

https://doi.org/10.1021/acs.chemmater.3c01220
Chem. Mater. 2023, 35, 5648−5656

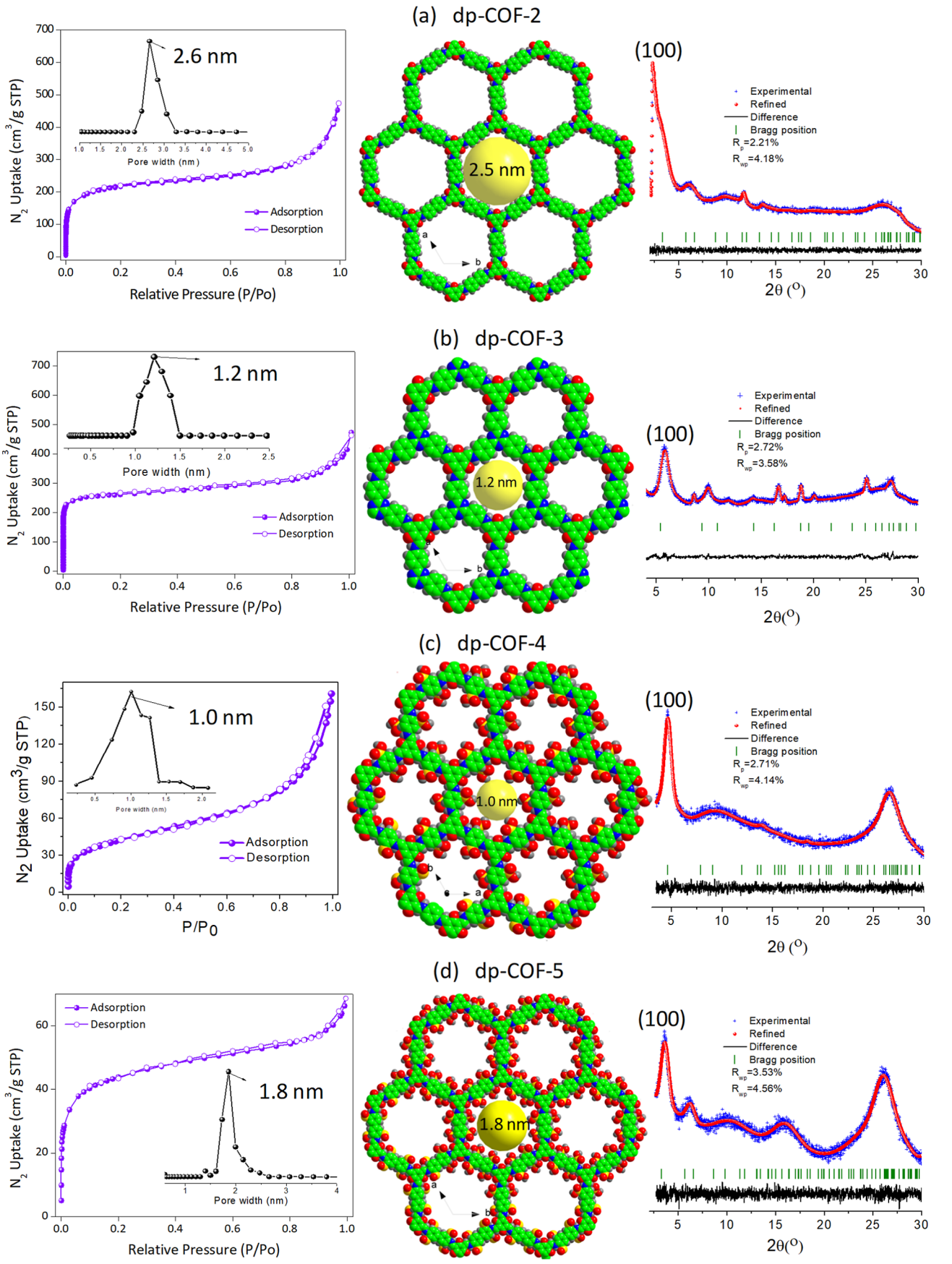

Figure 3. (a–d) N_2 adsorption–desorption isotherms with the inset of the pore size distribution, structures, and PXRD studies for dpCOF-*n* (*n* = 2–5).

https://doi.org/10.1021/acs.chemmater.3c01220
Chem. Mater. 2023, 35, 5648–5656

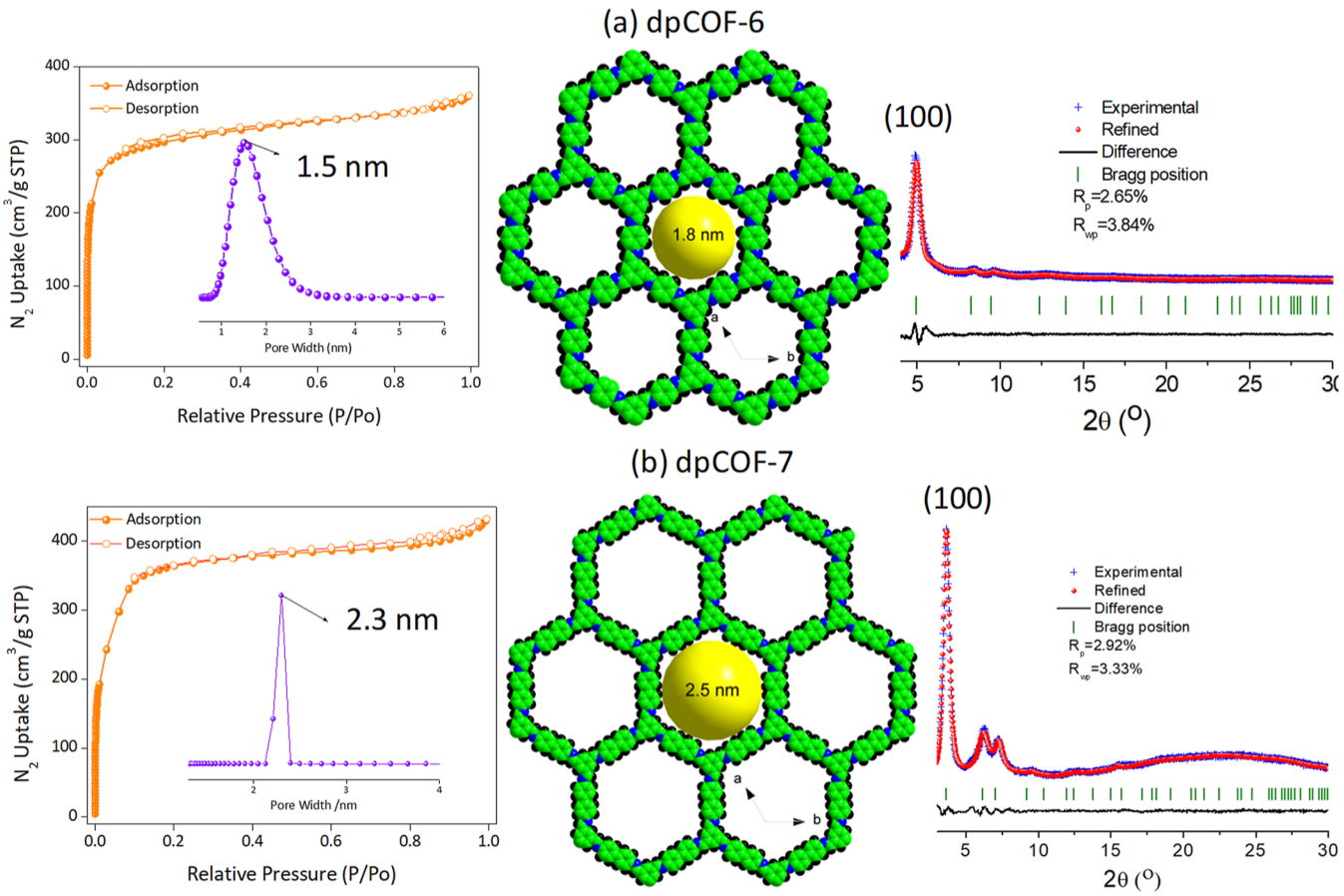

Figure 4. (a,b) N_2 adsorption−desorption isotherms with the inset of the pore size distribution, structures, and PXRD studies for dpCOF-*n* (*n* = 6−7).

water also showed a positive relationship with the consumed amount of imidazole. For example, nearly no dissolution was observed in the absence of imidazole, while little dissolution and partial dissolution was observed by the use of 0.15 and 0.75 mmol imidazole, respectively. By contrast, completely dissolved solution could be only obtained by consumption of 2 mmol imidazole. The foregoing results strongly suggest the key effect from imidazole on accelerating not only the dissolution of organic monomers in water but also the Schiff base reaction for production of dpCOF-1. More impressively, as we know, addition of acetic acid has been an essential prerequisite in previously reported synthesis of COFs through the Schiff base reaction involved in both solvothermal and water syntheses. By contrast, acetic acid can be avoided only in our synthesis procedure.

3.4. Large-Scale Synthesis of dpCOF-1. More importantly, large-scale synthesis of dpCOF-1 can also be implemented. In a typical synthesis process, gram-scale products of dpCOF-1 from one batch reaction were obtained as follows. The completely dissolved solution was obtained through stirring the aqueous solution containing A1(6 mmol), T(4 mmol), and imidazole (30 mmol) for 5 min at room temperature, while formation of dpCOF-1 was immediately finished by adding CH_3OH into this solution, giving 1.4 g products. The porosity of the as-synthesized gram-scale samples was confirmed by N_2 adsorption, giving a comparable adsorption isotherm as observed in the small-scale samples (Figure 2f).

3.5. Generality in the Synthesis of Ketoenamine-Linked COFs. To demonstrate the generality of an imidazole-accelerating aqueous synthesis strategy, we further synthesized other four ketoenamine-linked COFs using amino monomers of benzidine (A2), 4,4′,4″-(1,3,5-triazine-2,4,6-triyl)trianiline (A3), 2,5-diaminobenzenesulfonic acid (A4), and 4,4′-diamino-[1,1′-biphenyl]-3,3′-disulfonic acid (A5), respectively. Correspondingly, the resultant COFs were named dpCOF-2, dpCOF-3, dpCOF-4, and dpCOF-5, respectively. Their structures were revealed by a series of characterizations including IR (Figures S8−S11), solid-state ^{13}C NMR spectra (Figures S12−S15), SEM−EDS (Figures S16−S19), N_2 adsorption, PXRD, and structural refinement (Figure 3). The obtained results revealed a ketoenamine-linked framework with AA eclipsed stacking models for these dpCOFs. The BET surface areas for dpCOF-*n* (*n* = 2−5) are 794, 1019, 147, and 160 m^2/g, respectively. Remarkably, synthesis of sulfonic-anchored COFs using a monomer of A4 and A5 in previous reports must require 6 or 12 M acetic acid to catalyze Schiff base reaction.[30,31] By contrast, our approach represents the first preparation of crystalline sulfonic-anchored COFs without acetic acid.

3.6. Extending in the Synthesis of Imine-Bridged COFs. In addition, to extend its application scope, we further investigated the synthesis of imine-bridged COFs by our DP approach, and two imine-bridged COFs, dpCOF-6 and dpCOF-7, were representatively prepared. Their structure, crystallinity, and porosity was also confirmed by IR (Figures S20−S21), solid-state ^{13}C NMR spectra (Figures S22−S23),

https://doi.org/10.1021/acs.chemmater.3c01220
Chem. Mater. 2023, 35, 5648−5656

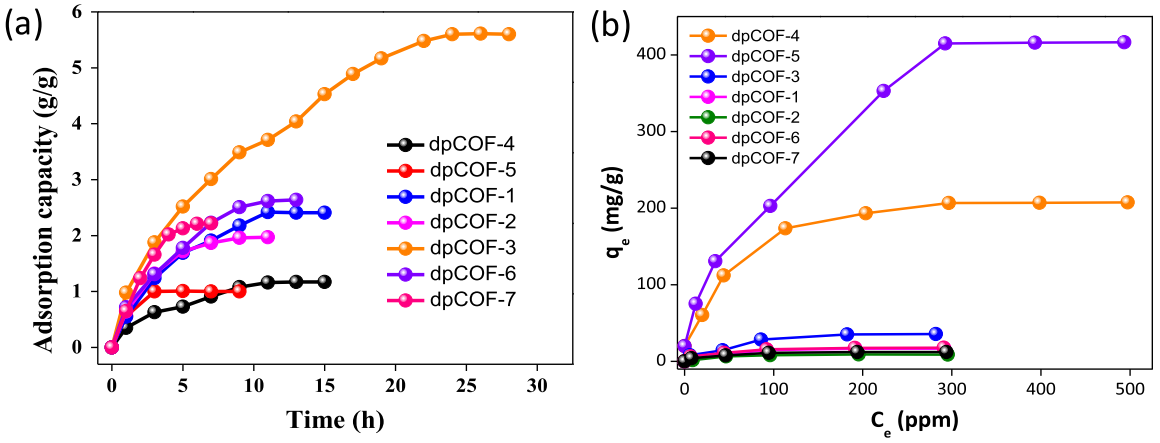

Figure 5. I_2/above and UO_2^{2+}/below capture upon these dpCOFs.

PXRD, and N_2 adsorption tests (Figure 4). IR peaks at 1614 cm^{-1} in both dpCOF-6 and dpCOF-7 confirmed the formation of imine bands; and this can be further attested in the solid-state ^{13}C NMR spectra with a peak around 160 ppm (belonging to the carbon atom from the C═N bond). Intense PRXD patterns at $2\theta < 5°$ implied high crystallinity in both dpCOF-6 and dpCOF-7. Impressively, their porosity reflected by BET surface areas were as high as 1110 and 1342 m^2/g, respectively. The foregoing results confirmed the success in the synthesis of imine-bridged COFs by our DP approach, and our DP method seems more facile for the preparation of imine-bridged COFs, as evidenced by the higher BET surface area, relative to ketoenamine-linked COFs, such as dpCOF-1 and dpCOF-2.

3.7. Mechanization of Such DP Method. Imidazole is viewed to be an excellent hydrogen-bonding building block (both hydrogen donor and hydrogen acceptor) and usually shows weak acidity in water. Thus, fixing both aldehyde and amino monomers around imidazole molecules through hydrogen-bonded interactions could be expected; and this finally leads to the complete dissolution of both aldehyde and amino monomers in water in the dissolution step. At the same time, the weak acidity of imidazole could catalyze the Schiff base reaction with the formation of ketoenamine- or imine linkages. Different from the all established water-synthesis methods with the formation of COFs in water,[25−28] our approach does not directly generate COFs in water but just with the formation of the crucial factor, such as the ketoenamine- or imine linkages. This could avoid the rapid and poor crystallization in water, as observed in the literature.[25−28]

To crystallize the COF from the completely dissolved solution, we herein used CH_3OH as a precipitant in the precipitation step. As we know, CH_3OH can be miscible with water through hydrogen bonds; and this could be expected to give a significant effect on the solubility of organic monomers in water, thus inducing the rapid, large-scale, and high-quality crystallization of COFs in the water/methanol mixture.

3.8. Radionuclide Removal. In light of their large-scale and simple synthesis of COFs, we made an initial attempt in industrial applications for I_2 and UO_2^{2+} capture. As shown in Figure 5, these materials afforded the uptake capacity of I_2 with the hierarchy, dpCOF-3 (5.6 g/g) > dpCOF-6 (2.6 g/g) > dpCOF-1 (2.4 g/g) > dpCOF-7 (2.2 g/g) > dpCOF-2 (1.9 g/g) > dpCOF-4 (1.2 g/g) > dpCOF-5 (1.0 g/g). The results imply that nitrogen-rich COFs avails to I_2 capture, as evidenced by the outstanding I_2 uptake in dpCOF-3 over other dpCOFs. Moreover, the adsorption rate of iodine is also very important for practical applications, which is usually defined by $K_{80\%}$.[32−34] For example, dpCOF-3 affords a $K_{80\%}$ of 0.26 g/h. Notably, both the uptake capacity and adsorption rate in dpCOF-3 is comparable with the most reported I_2 adsorbents.[35,36]

On the other hand, UO_2^{2+} capture gave the hierarchy, dpCOF-5 (416 mg/g) > dpCOF-4 (207 mg/g) > dpCOF-3 (36 mg/g) > dpCOF-1 (17 mg/g) > dpCOF-2 (9 mg/g) > dpCOF-6 (18 mg/g) > dpCOF-7 (12 mg/g) (Figure 5). The high UO_2^{2+} capture in dpCOF-5 and dpCOF-4 is due to the coordination interactions from free-standing sulfonic units, while the low UO_2^{2+} capture in dpCOF-*n* (1−3) is due to the absence of adsorption site in these COFs. The adsorption isotherms of dpCOF-5 and dpCOF-4 can be well fitted by the Langmuir model (Table S1). The uptake capacity in dpCOF-5 is comparable with some remarkable UO_2^{2+} adsorbents.[37−40] In IR spectra, the peak at 928 cm^{-1} in dpCOF-4 and dpCOF-5 was assigned to the antisymmetric vibration of uranyl ions (Figure S24).[41] In contrast to $UO_2(NO_3)_2{\cdot}6H_2O$ with peaks at 960 cm^{-1}, the big red shift for the samples after the UO_2^{2+} uptake indicates strong coordination interactions between sulfonic units and uranyl ions.[41]

The low-cost and large-scale synthesis in conjunction with the high radionuclide adsorption performance in dpCOF-3 and dpCOF-5 suggests their superior applications in uranium recovery from spent fuel and iodine removal from radioactive off-gas.[32−43]

4. CONCLUSIONS

In summary, we demonstrate a proof-of-concept of synthesis of ketoenamine- and imine-linked COFs via a two-step DP strategy. We systematically studied this method including preparation of model compounds, effect from the consumed amount of imidazole on the COF synthesis, large-scale synthesis, and generality in synthesis of COFs. Upon this DP route, we can expediently prepare COF materials within 5 min by simply stirring these organic monomers in water at room temperature without acetic acid catalysis, allowing more facile methods than the established methods such as solvothermal, hydrothermal, mechanochemical, solid-state, and sonochemical syntheses. These outstanding advantages make our DP route more suitable and accessible for expanding COF synthesis and industrial applications.

https://doi.org/10.1021/acs.chemmater.3c01220
Chem. Mater. 2023, 35, 5648−5656

■ ASSOCIATED CONTENT

Supporting Information

The Supporting Information is available free of charge at https://pubs.acs.org/doi/10.1021/acs.chemmater.3c01220.

Synthesis of model compounds, characterizations, adsorption experiments of UO_2^{2+} and I_2 in detail, structures of model compounds, PXRD data, IR data, SEM images, solid-state ^{13}C NMR spectra, and fitting results by the Langmuir model (PDF)

■ AUTHOR INFORMATION

Corresponding Authors

Zhiwu Yu − *High Magnetic Field Laboratory Chinese Academy of Sciences, Hefei, Anhui 230031, China*; Email: zhiwuyu@hmfl.ac.cn

Feng Luo − *School of Chemistry, Biology and Materials Science, East China University of Technology, Nanchang 330013, China*; orcid.org/0000-0001-6380-2754; Email: ecitluofeng@163.com

Authors

Liecheng Guo − *School of Chemistry, Biology and Materials Science, East China University of Technology, Nanchang 330013, China*

Qing Yun Zhang − *School of Chemistry, Biology and Materials Science, East China University of Technology, Nanchang 330013, China*

Rajamani Krishna − *Van't Hoff Institute for Molecular Sciences, University of Amsterdam, Amsterdam 1098 XH, The Netherlands*; orcid.org/0000-0002-4784-8530

Complete contact information is available at: https://pubs.acs.org/10.1021/acs.chemmater.3c01220

Notes

The authors declare no competing financial interest.

■ ACKNOWLEDGMENTS

This work was supported financially by the National Natural Science Foundations of China (21966002, 42177444, and U1932218), the Youth leading talent project of FuZhou (NO.2020ED64), and the Jiangxi project (DHSQT22021007). The authors would also like to thank Wenqian Liu from Shiyanjia Lab (www.Shiyanjia.com) for the XRD analysis.

■ REFERENCES

(1) Côté, A. P.; Benin, A. I.; Ockwig, N. W.; O'Keeffe, M.; Matzger, A. J.; Yaghi, O. M. Porous, crystalline, covalent organic frameworks. *Science* **2005**, *310*, 1166−1170.

(2) Geng, K.; He, T.; Liu, R.; Dalapati, S.; Tan, K. T.; Li, Z.; Tao, S.; Gong, Y.; Jiang, Q.; Jiang, D. Covalent organic frameworks: design, synthesis, and functions. *Chem. Rev.* **2020**, *120*, 8814−8933.

(3) Kandambeth, S.; Dey, K.; Banerjee, R. Covalent organic frameworks: chemistry beyond the structure. *J. Am. Chem. Soc.* **2019**, *141*, 1807−1822.

(4) Li, H.; Chen, F.; Guan, X.; Li, J.; Li, C.; Tang, B.; Valtchev, V.; Yan, Y.; Qiu, S.; Fang, Q. Three-dimensional triptycene-based covalent organic frameworks with ceq or acs topology. *J. Am. Chem. Soc.* **2021**, *143*, 2654−2659.

(5) Ahmad, N.; Chughtai, A. H.; Younus, H. A.; Verpoort, F. Discrete metal-carboxylate self-assembled cages: design, synthesis and applications. *Coord. Chem. Rev.* **2014**, *280*, 1−27.

(6) Wang, D.; Qiu, T.; Guo, W.; Liang, Z.; Tabassum, H.; Xia, D.; Zou, R. Covalent organic framework-based materials for energy applications. *Energy Environ. Sci.* **2021**, *14*, 688−728.

(7) Wang, Z.; Zhang, S.; Chen, Y.; Zhang, Z.; Ma, S. Covalent organic frameworks for separation applications. *Chem. Soc. Rev.* **2020**, *49*, 708−735.

(8) Waller, P. J.; Gándara, F.; Yaghi, O. M. Chemistry of covalent organic frameworks. *Acc. Chem. Res.* **2015**, *48*, 3053−3063.

(9) Ding, S. Y.; Wang, W. Covalent organic frameworks (COFs): from design to applications. *Chem. Soc. Rev.* **2013**, *42*, 548−568.

(10) Wang, S.; Wang, Q.; Shao, P.; Han, Y.; Gao, X.; Ma, L.; Yuan, S.; Ma, X.; Zhou, J.; Feng, X.; Wang, B. Exfoliation of covalent organic frameworks into few-layer redox-active nanosheets as cathode materials for Lithium-ion batteries. *J. Am. Chem. Soc.* **2017**, *139*, 4258−4261.

(11) Zhang, J.; Han, X.; Wu, X.; Liu, Y.; Cui, Y. Multivariate chiral covalent organic frameworks with controlled crystallinity and stability for asymmetric catalysis. *J. Am. Chem. Soc.* **2017**, *139*, 8277−8285.

(12) Gao, C.; Li, J.; Yin, S.; Lin, G.; Ma, T.; Meng, Y.; Sun, J.; Wang, C. Isostructural three-dimensional covalent organic frameworks. *Angew. Chem., Int. Ed.* **2019**, *58*, 9770−9775.

(13) Guan, X.; Li, H.; Ma, Y.; Xue, M.; Fang, Q.; Yan, Y.; Valtchev, V.; Qiu, S. Chemically stable polyarylether-based covalent organic frameworks. *Nat. Chem.* **2019**, *11*, 587−594.

(14) Bi, S.; Yang, C.; Zhang, W.; Xu, J.; Liu, L.; Wu, D.; Wang, X.; Han, Y.; Liang, Q.; Zhang, F. Two-dimensional semiconducting covalent organic frameworks via condensation at arylmethyl carbon atoms. *Nat. Commun.* **2019**, *10*, 2467.

(15) Yuan, C.; Fu, S.; Yang, K.; Hou, B.; Liu, Y.; Jiang, J.; Cui, Y. Crystalline C—C and C=C Bond-Linked Chiral Covalent Organic Frameworks. *J. Am. Chem. Soc.* **2021**, *143*, 369−381.

(16) Wang, Z.; Yang, Y.; Zhao, Z.; Zhang, P.; Zhang, Y.; Liu, J.; Ma, S.; Cheng, P.; Chen, Y.; Zhang, Z. Green synthesis of olefin-linked covalent organic frameworks for hydrogen fuel cell applications. *Nat. Commun.* **2021**, *12*, 1982.

(17) Meng, F.; Bi, S.; Sun, Z.; Wu, D.; Zhang, F. 2,4,6-Trimethylpyridine-derived vinylene-linked covalent organic frameworks for confined catalytic esterification. *Angew. Chem., Int. Ed.* **2022**, *61*, No. e202210447.

(18) Campbell, N. L.; Clowes, R.; Ritchie, L. K.; Cooper, A. I. Rapid microwave synthesis and purification of porous covalent organic frameworks. *Chem. Mater.* **2009**, *21*, 204−206.

(19) Matsumoto, M.; Dasari, R. R.; Ji, W.; Feriante, C. H.; Parker, T. C.; Marder, S. R.; Dichtel, W. R. Rapid, low temperature formation of imine-linked covalent organic frameworks catalyzed by metal triflates. *J. Am. Chem. Soc.* **2017**, *139*, 4999−5002.

(20) Zhang, M.; Chen, J.; Zhang, S.; Zhou, X.; He, L.; Sheridan, M. V.; Yuan, M.; Zhang, M.; Chen, L.; Dai, X.; Ma, F.; Wang, J.; Hu, J.; Wu, G.; Kong, X.; Zhou, R.; Albrecht-Schmitt, T. E.; Chai, Z.; Wang, S. Electron beam irradiation as a general approach for the rapid synthesis of covalent organic frameworks under ambient conditions. *J. Am. Chem. Soc.* **2020**, *142*, 9169−9174.

(21) Biswal, B. P.; Chandra, S.; Kandambeth, S.; Lukose, B.; Heine, T.; Banerjee, R. Mechanochemical synthesis of chemically stable isoreticular covalent organic frameworks. *J. Am. Chem. Soc.* **2013**, *135*, 5328−5331.

(22) Karak, S.; Kandambeth, S.; Biswal, B. P.; Sasmal, H. S.; Kumar, S.; Pachfule, P.; Banerjee, R. Constructing ultraporous covalent organic frameworks in seconds via an organic terracotta process. *J. Am. Chem. Soc.* **2017**, *139*, 1856−1862.

(23) Lan, Z.; Wu, M.; Fang, Z.; Zhang, Y.; Chen, X.; Zhang, G.; Wang, X. Ionothermal synthesis of covalent triazine frameworks in a NaCl-KCl-$ZnCl_2$ eutectic salt for the hydrogen evolution reaction. *Angew. Chem., Int. Ed.* **2022**, *61*, No. e202201482.

(24) Bi, S.; Meng, F.; Wu, D.; Zhang, F. Synthesis of vinylene-linked covalent organic frameworks by monomer self-catalyzed activation of knoevenagel condensation. *J. Am. Chem. Soc.* **2022**, *144*, 3653−3659.

(25) Guan, X.; Ma, Y.; Li, H.; Yusran, Y.; Xue, M.; Fang, Q.; Yan, Y.; Valtchev, V.; Qiu, S. Fast, ambient temperature and pressure

ionothermal synthesis of three-dimensional covalent organic frameworks. *J. Am. Chem. Soc.* **2018**, *140*, 4494−4498.
(26) Thote, J.; Barike Aiyappa, H.; Rahul Kumar, R.; Kandambeth, S.; Biswal, B. P.; Balaji Shinde, D.; Chaki Roy, N.; Banerjee, R. Constructing covalent organic frameworks in water via dynamic covalent bonding. *IUCrJ* **2016**, *3*, 402−407.
(27) Lu, J.; Lin, F.; Wen, Q.; Qi, Q. Y.; Xu, J. Q.; Zhao, X. Large-scale synthesis of azine-linked covalent organic frameworks in water and promoted by water. *New J. Chem.* **2019**, *43*, 6116−6120.
(28) Martín-Illán, J. Á.; Rodríguez-San-Miguel, D.; Franco, C.; Imaz, I.; Maspoch, D.; Puigmartí-Luis, J.; Zamora, F. Green synthesis of imine-based covalent organic frameworks in water. *Chem. Commun.* **2020**, *56*, 6704−6707.
(29) Zhao, W.; Yan, P.; Yang, H.; Bahri, M.; James, A. M.; Chen, H.; Liu, L.; Li, B.; Pang, Z.; Clowes, R.; Browning, N. D.; Ward, J. W.; Wu, Y.; Cooper, A. I. Using sound to synthesize covalent organic frameworks in water. *Nat. Synth.* **2022**, *1*, 87−95.
(30) Xiong, X.; Yu, Z.; Gong, L.; Tao, Y.; Gao, Z.; Wang, L.; Yin, W.; Yang, L.; Luo, F. Ammoniating covalent organic framework (COF) for high-performance and selective extraction of toxic and radioactive uranium ions. *Adv. Sci.* **2019**, *6*, 1900547.
(31) Zhang, Q.; Dong, S.; Shao, P.; Zhu, Y.; Mu, Z.; Sheng, D.; Zhang, T.; Jiang, X.; Shao, R.; Ren, Z.; Xie, J.; Feng, X.; Wang, B. Covalent organic framework−based porous ionomers for high-performance fuel cells. *Science* **2022**, *378*, 181−186.
(32) Guo, X. H.; Li, Y.; Zhang, M. C.; Cao, K. C.; Tian, Y.; Qi, Y.; Li, S. J.; Li, K.; Yu, X. Q.; Ma, L. J. Colyliform crystalline 2D covalent organic frameworks (COFs) with quasi-3D topologies for rapid I_2 adsorption. *Angew. Chem., Int. Ed.* **2020**, *59*, 22697−22705.
(33) Xie, Y. Q.; Pan, T. T.; Lei, Q.; Chen, C. L.; Dong, X. L.; Yuan, Y. Y.; Shen, J.; Cai, Y. C.; Zhou, C. H.; Pinnau, I.; Han, Y. Ionic functionalization of multivariate covalent organic frameworks to achieve an exceptionally high iodine-capture capacity. *Angew. Chem., Int. Ed.* **2021**, *60*, 22432−22440.
(34) He, L. W.; Chen, L.; Dong, X. L.; Zhang, S. T.; Zhang, M. X.; Dai, X.; Liu, X. J.; Lin, P.; Li, K. F.; Chen, C. L.; Pan, T. T.; Ma, F. Y.; Chen, J. C.; Yuan, M. J.; Zhang, Y. G.; Chen, L.; Zhou, R. H.; Han, Y.; Chai, Z. F.; Wang, S. A. A nitrogen-rich covalent organic framework for simultaneous dynamic capture of iodine and methyl iodide. *Chem* **2021**, *7*, 699−714.
(35) Huang, Y. W.; Yu, Z. W.; Zhang, Q. Y.; Luo, F. Constructing quinazolinone-anchored electron-rich covalent organic frameworks by photocatalytic reductive cyclization for idealizing iodine capture. *Sci. China Mater.* **2023**, *66*, 2339−2345.
(36) Xie, Y. Q.; Pan, T. T.; Lei, Q.; Chen, C. L.; Dong, X. L.; Yuan, Y. Y.; Maksoud, W. A.; Zhao, L.; Cavallo, L.; Pinnau, I.; Han, Y. Efficient and simultaneous capture of iodine and methyl iodide achieved by a covalent organic framework. *Nat. Commun.* **2022**, *13*, 2878.
(37) Sun, Q.; Aguila, B.; Perman, J.; Ivanov, A. S.; Bryantsev, V. S.; Earl, L. D.; Abney, C. W.; Wojtas, L. S.; Ma, S. Bio-inspired nano-traps for uranium extraction from seawater and recovery from nuclear waste. *Nat. Commun.* **2018**, *9*, 1644.
(38) Zhang, H.; Liu, W.; Li, A.; Zhang, D.; Li, X.; Zhai, F.; Chen, L.; Chen, L.; Wang, Y.; Wang, S. Three mechanisms in one material: uranium capture by a polyoxometalate−organic framework through combined complexation, chemical reduction, and photocatalytic reduction. *Angew. Chem., Int. Ed.* **2019**, *58*, 16110−16114.
(39) Abney, C. W.; Mayes, R. T.; Saito, T.; Dai, S. Materials for the recovery of uranium from seawater. *Chem. Rev.* **2017**, *117*, 13935−14013.
(40) Dai, S. Catalyst: Challenges in development of adsorbents for recovery of uranium from seawater. *Chem* **2021**, *7*, 537−539.
(41) Xu, Y.; Yu, Z. W.; Zhang, Q. Y.; Luo, F. Sulfonic-pendent vinylene-linked covalent organic frameworks enabling benchmark potential in advanced energy. *Adv. Sci.* **2023**, *10*, 2300408.
(42) He, L.; Li, B.; Ma, Z.; Chen, L.; Gong, S.; Zhang, M.; Bai, Y.; Guo, Q.; Wu, F.; Zhao, F.; Li, J.; Zhang, D.; Sheng, D.; Dai, X.; Chen, L.; Shu, J.; Chai, Z.; Wang, S. Synergy of first- and second-sphere interactions in a covalent organic framework boosts highly selective platinum uptake. *Sci. China: Chem.* **2023**, *66*, 783−790.
(43) Bai, Y.; Chen, L.; He, L.; Li, B.; Chen, L.; Wu, F.; Chen, L.; Zhang, M.; Liu, Z.; Chai, Z.; Wang, S. Precise recognition of palladium through interlaminar chelation in a covalent organic framework. *Chem* **2022**, *8*, 1442−1459.

https://doi.org/10.1021/acs.chemmater.3c01220
Chem. Mater. 2023, 35, 5648−5656

Minute and Large-Scale Synthesis of Covalent-Organic Framework in Water at Room Temperature by a Two-Step Dissolution-Precipitation Method

Liecheng Guo,[a] Qing Yun Zhang,[a] Zhiwu Yu,[b]* Rajamani Krishna,[c] and Feng Luo[a]*
Corresponding author, ecitluofeng@163.com (F. L.) and zhiwuyu@hmfl.ac.cn (Z. Y.)

Experimental section

Materials and general methods

Reagents and solvents were commercially available (Alfa) and were used without further purification. X-ray powder diffraction were collected by a Bruker AXSD8 Discover powder diffractometer at 40 kV, 40 mA for Cu Kλ (λ= 1.5406 Å). The simulated powder patterns were calculated by Mercury 1.4. Infrared Spectra (IR) were measured by a Bruker VERTEX70 spectrometer in the 800-3600 cm^{-1} region. The gas adsorption isotherms were collected on a Belsorp-max. Ultrahigh-purity-grade (>99.999%) N_2 gases were used during the adsorption measurement. SEM and EDS measurements were carried out using a Hitachi S-4800 microscope. The analyses of concentrations of UO_2^{2+} ions in the solution was carried out by ThermoFisher iCap7600 ICP-OES instruments. Solid-state NMR experiments were performed on Varian Infinityplus 300 solid-state NMR spectrometer (300MHz).

Synthesis

Synthesis of model compound (I)

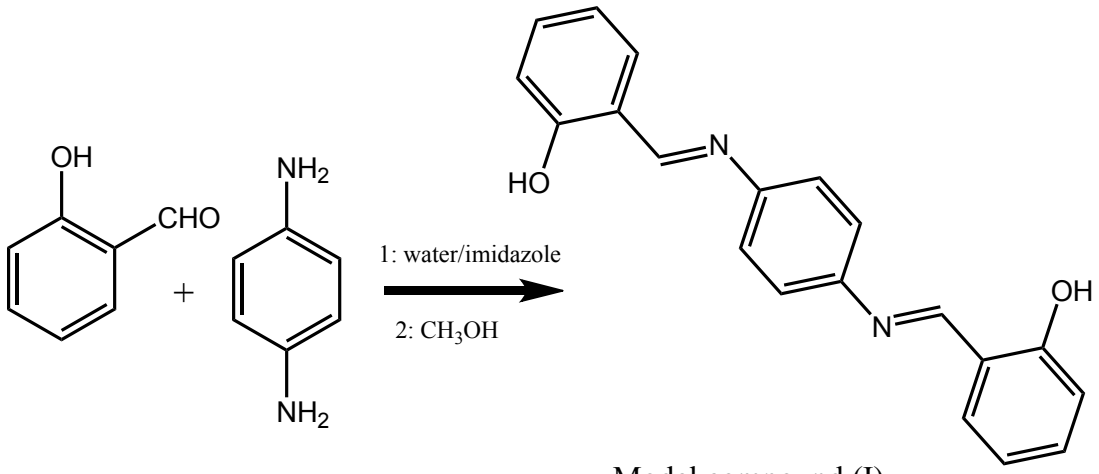

Model compound (I)

Model compound (I) was prepared as follows. A mixture of 2-hydroxybenzaldehyde (48.8 uL, 0.4 mmol), benzene-1,4-diamine (42 mg, 0.2 mmol), and imidazole (100 mg, 1.5 mmol) was mixed in a beaker (10 mL) in 2 mL water, then it was stirred for 5 minutes, and a clear solution was observed. Adding 5 mL CH_3OH into the above solution will immediately regenerate a large number of precipitation. Big block crystals (yield of >98%) could be obtained through recrystallization from $CHCl_3$. Both ^1H nuclear magnetic resonance (NMR) and single-crystal X-ray diffraction were used to confirm the product and purity. ^1H NMR (400 MHz, Chloroform-d) δ(ppm) 8.57 (d, J = 27.3 Hz, 2H), 7.41 – 7.06 (m, 9H), 6.90 (ddt, J = 26.4, 18.8, 7.8 Hz, 4H), 6.65 (d, J = 8.0 Hz, 1H). Element analysis: exp. 76.38%, H/4.45%, N/8.95%; calc. C/76.42%, H/4.49%, N/8.92%.

Synthesis of model compound (II)

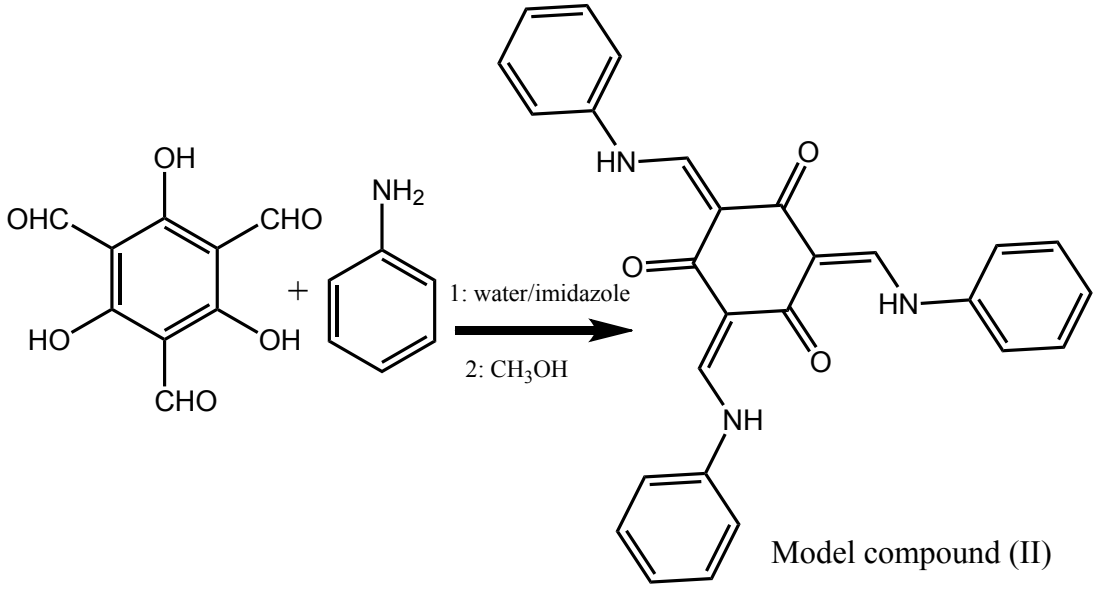

Model compound (II)

Model compound (II) was prepared as follows. A mixture of 2,4,6-trihydroxybenzene-1,3,5-tricarbaldehyde (42 mg, 0.2 mmol), aniline (56 uL, 0.3 mmol), and imidazole (100 mg, 1.5 mmol) was mixed in a beaker (10 mL) in 10 mL water, then it was stirred for 5 minutes, and a clear solution was observed. Adding 50 mL CH_3OH into the above solution will immediately regenerate a large number of precipitation. Very small block crystals (yield of >98%) could be obtained through recrystallization from $CHCl_3$. ^1H nuclear magnetic resonance (NMR) was used to confirm the product and purity. The very small block crystals could not be determined by single-crystal X-ray diffraction. ^1H NMR (500 MHz, Chloroform-d) δ(ppm) 8.95 – 8.42 (m, 3H), 7.63 – 6.87 (m, 15H). Element analysis: exp. 74.42%, H/4.83%, N/9.67%; calc. C/74.46%, H/4.86%, N/9.65%.

Uranium uptake *via* batch experiments

U(VI) solution was prepared by dissolving uranyl nitrate ($UO_2(NO_3)_2 \cdot 6H_2O$, analytical reagent) in deionized water. Adsorption temperature is 298 K. In a typical batch experiments, the U solution with initial concentration of 10-600 ppm and pH=5 was used. The dose of adsorbent is 10 mg, while the U solution is 20 mL and the contact time is 4 h.

The adsorption amount, Q_e (mg/g), was calculated by the difference of the U(VI) equilibrium concentration before and after adsorption (see equation 1):

$$Q_e = \frac{(C_0 - C_e) \times V}{m} \qquad (1)$$

where c_0 (mg/L) and c_e (mg/L) are the initial concentration and equilibrium concentration of uranium in the solutions, respectively; V (mL) is the volume of testing solution and m (mg) is the amount of sorbent.

Adsorption of I_2 vapor

Typically, two glass vials (2 mL) were placed in a wide-mouth jar (100 mL) containing I_2 (500 mg). Adsorbent (10 mg) was placed in the first vial, while the second one was used as a reference. Then, the wide-mouth jar was sealed and kept in a heated oven at 75°C. After a certain contact time, the wide-mouth jar was taken out and cooled to room temperature. The weight of the small vial containing the resulted sample was then measured. This procedure was terminated once the weight of resulted samples did not change, and the adsorption capacity (q_t, $g \cdot g^{-1}$) was experimentally measured by the weight increment of the resulted samples with the following equation (2):

$$q_t=[(m_t-m_1)-(M_t-M_0)]/(m_1-m_0) \quad (2)$$

where q_t ($g \cdot g^{-1}$) denotes the I_2 vapor capture uptake at time t, m_t (g) denotes the weight of the vial containing adsorbents at time t, m_1 (g) denotes the weight of the vial containing adsorbent before sorption, m_0 (g) denotes the weight of the empty vial for adsorbents, M_t (g) denotes the weight of the reference vial at time t, M_0 (g) denotes the weight of the reference vial before sorption.

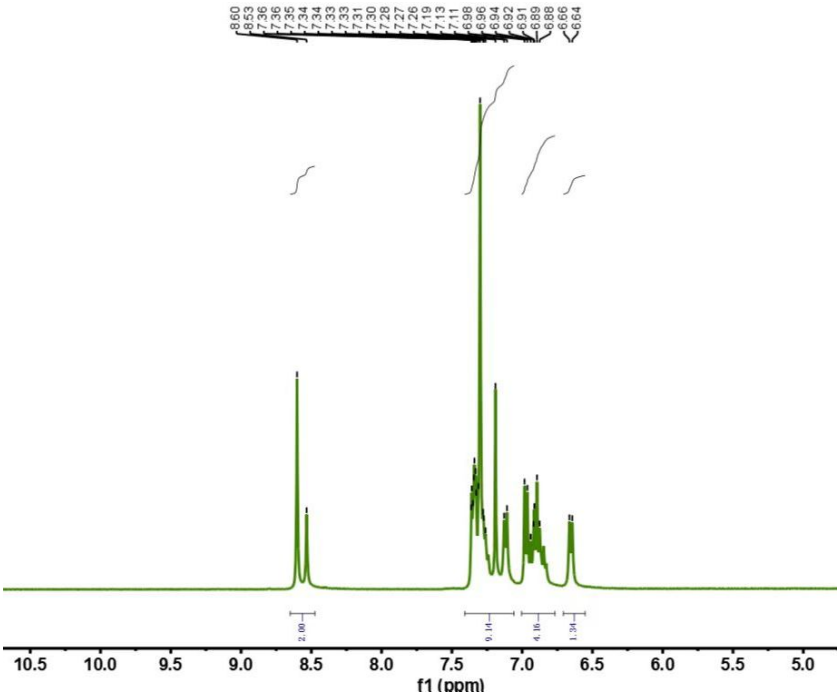

Figuer S1. The ^{1}H nuclear magnetic resonance (NMR) of model compound (I).

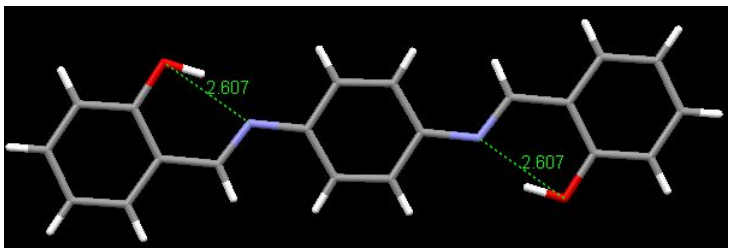

Figuer S2. View of the structure of model compound (I) with intra O-H…N hydrogen bonds.

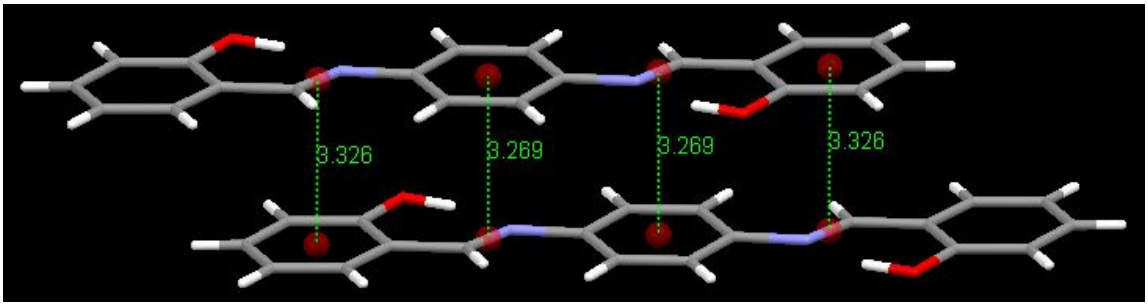

Figuer S3. View of the π-π stacking architecture in model compound (I).

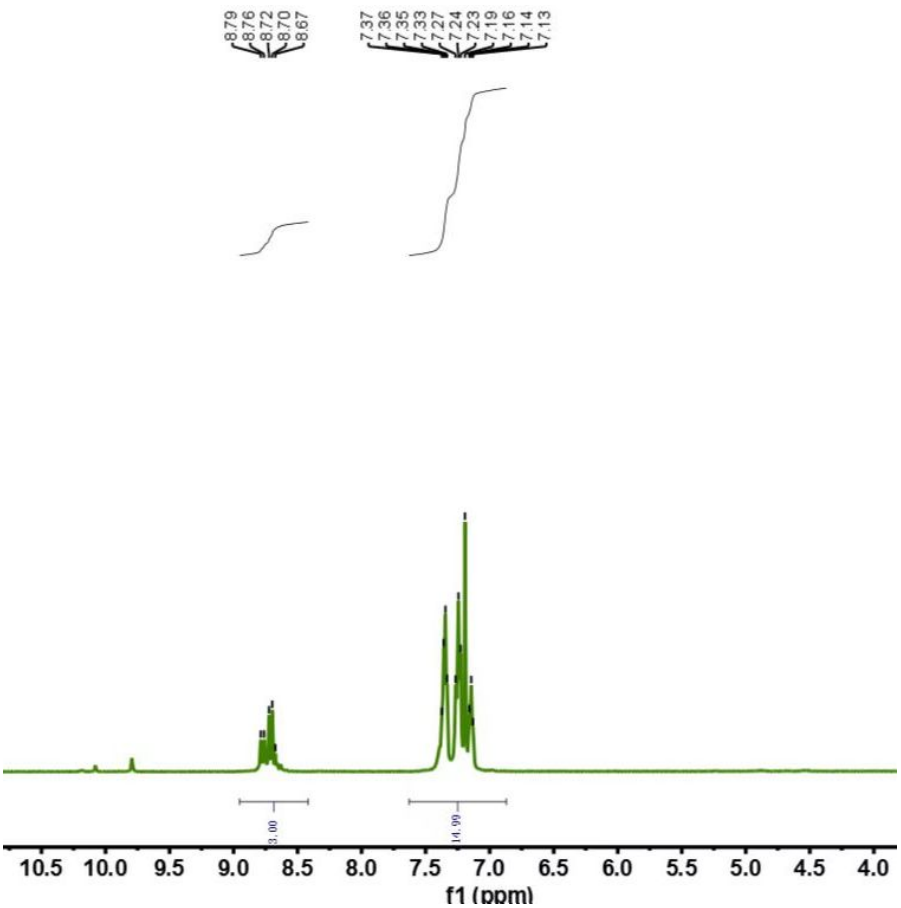

Figuer S4. The ^{1}H nuclear magnetic resonance (NMR) of model compound (II).

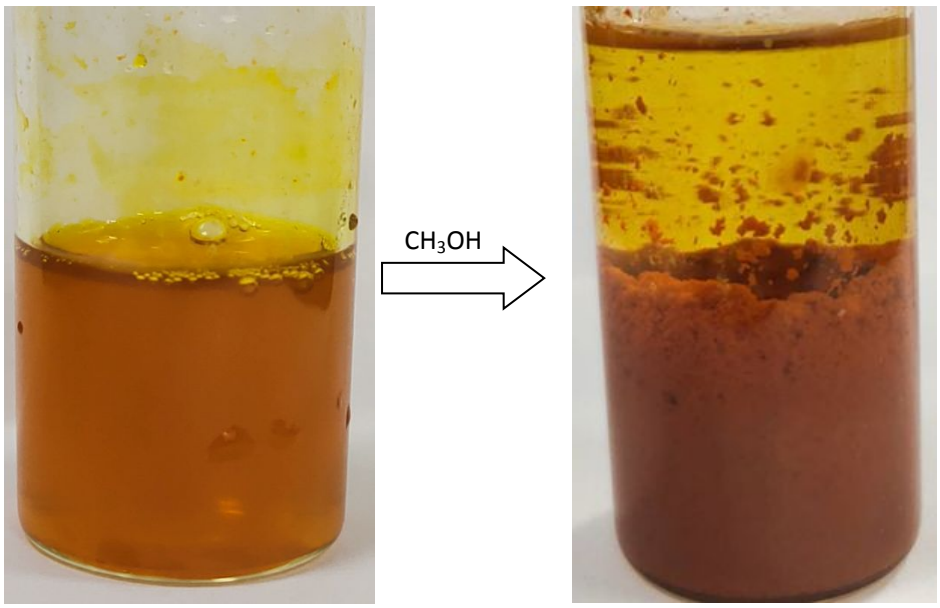

Figuer S5. The images of respectively dissolution and precipitation steps for the synthesis of dpCOF-1.

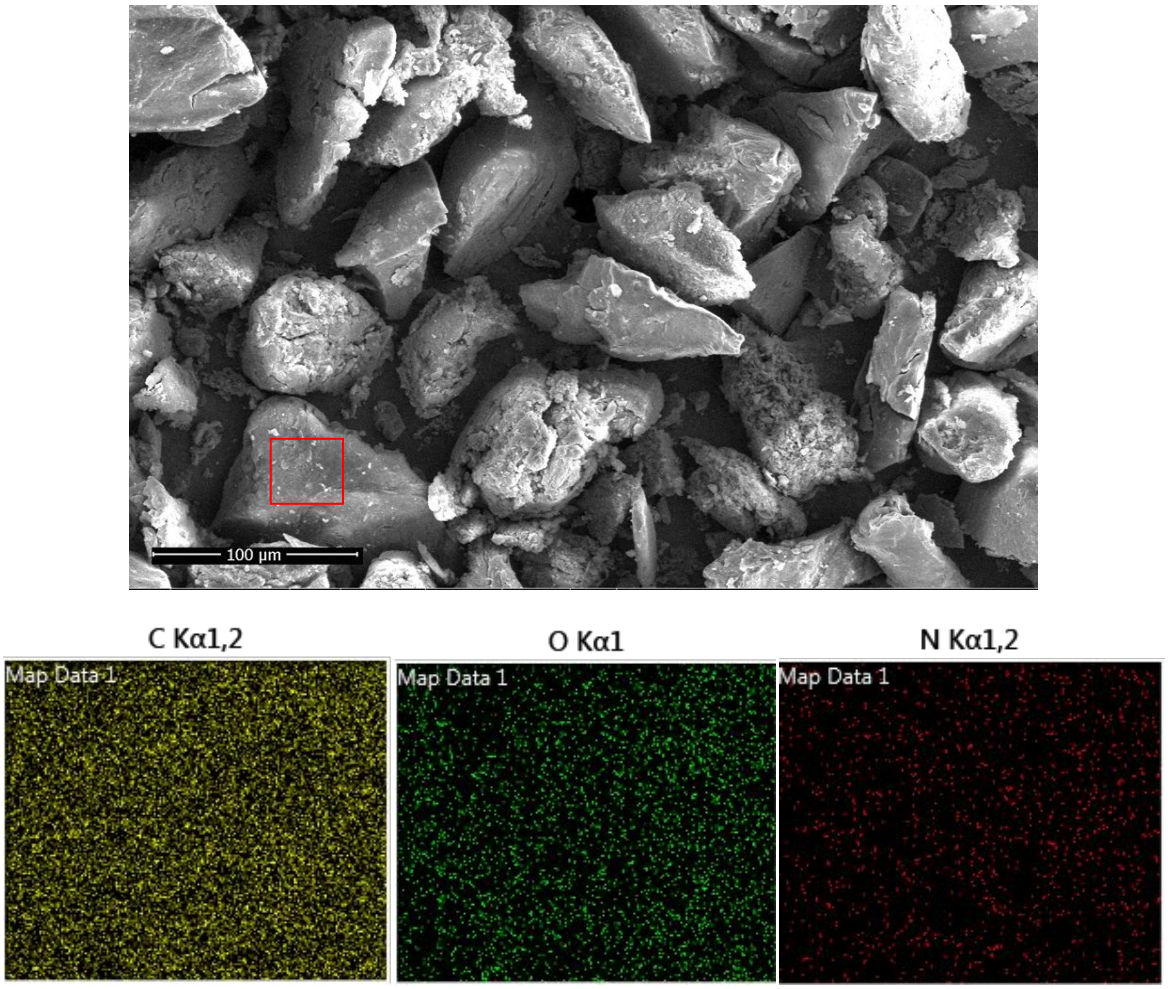

Figuer S6. The SEM image and EDS element mapping for dpCOF-1.

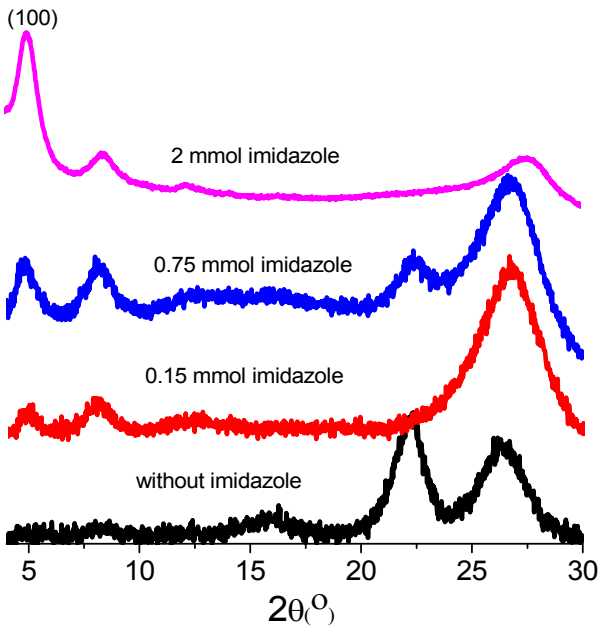

Figure S7. A comparison of PXRD patterns of the samples synthesized under various amount of imidazole.

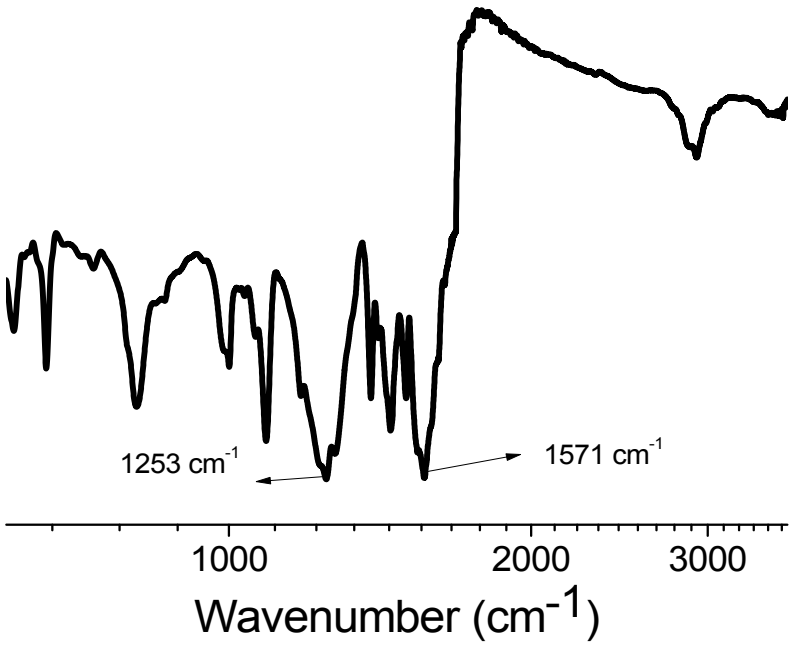

Figuer S8. The IR spectra of dpCOF-2.

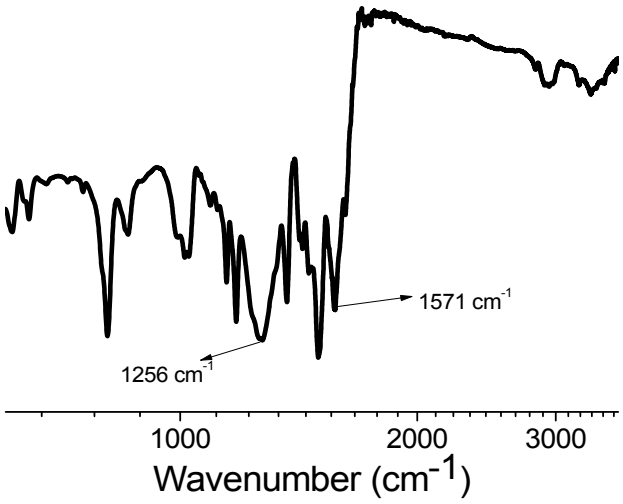

Figuer S9. The IR spectra of dpCOF-3.

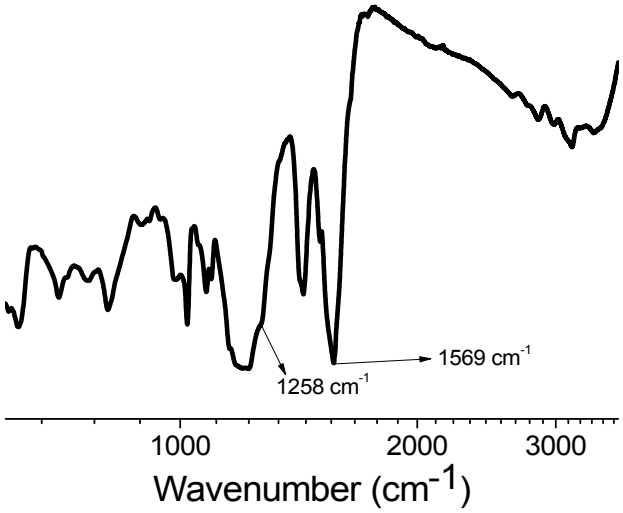

Figuer S10. The IR spectra of dpCOF-4.

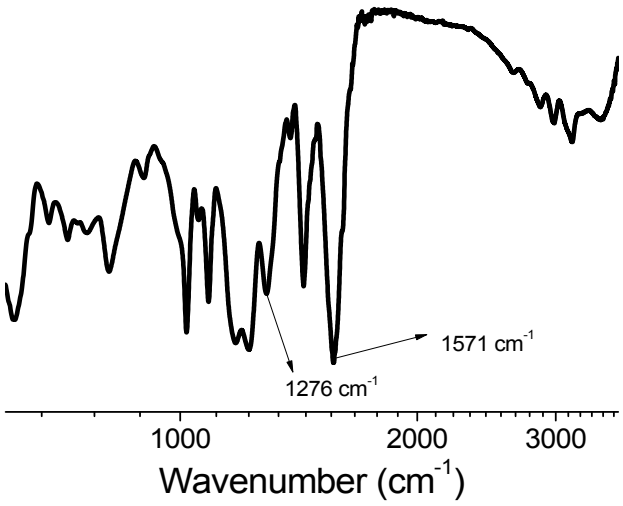

Figuer S11. The IR spectra of dpCOF-5.

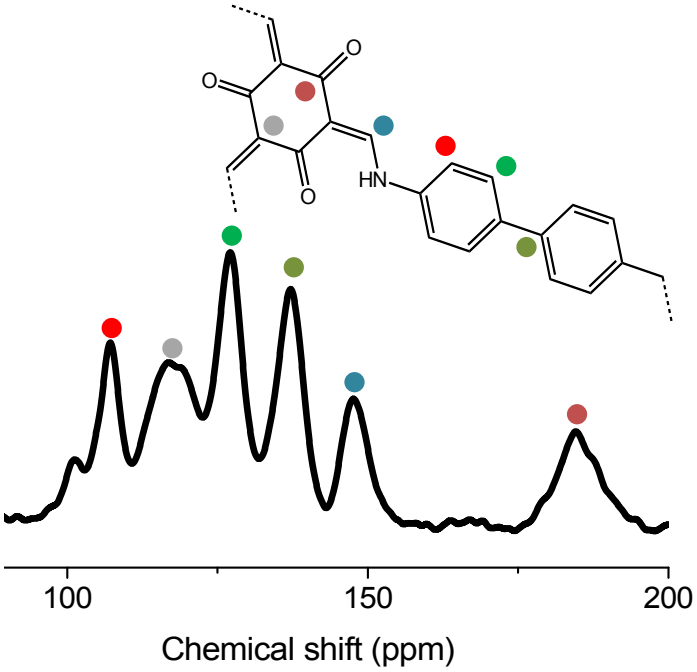

Figuer S12. Solid state ^{13}C NMR spectra of dpCOF-2.

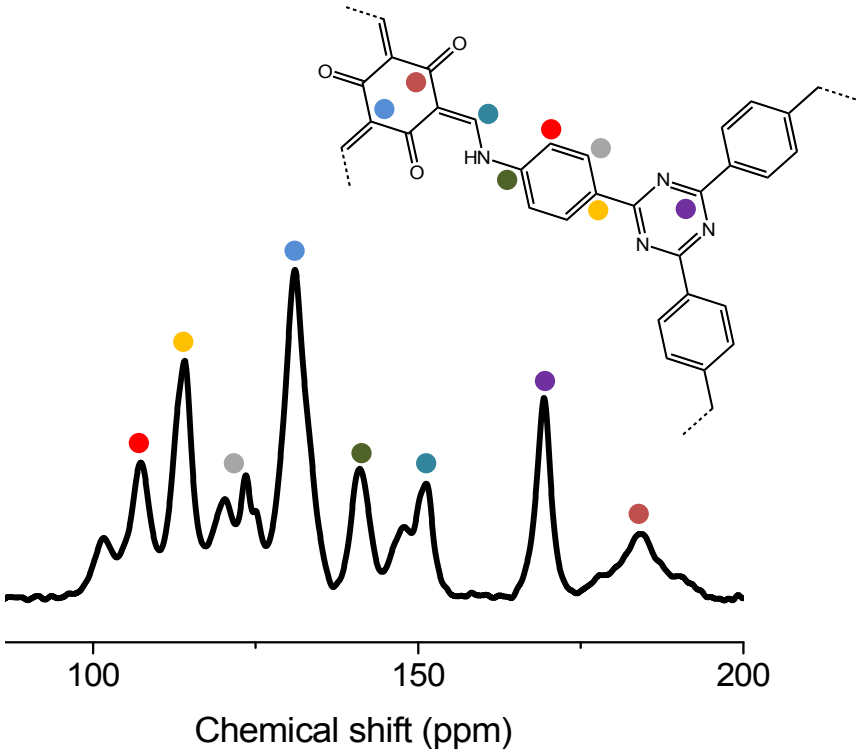

Figuer S13. Solid state ^{13}C NMR spectra of dpCOF-3.

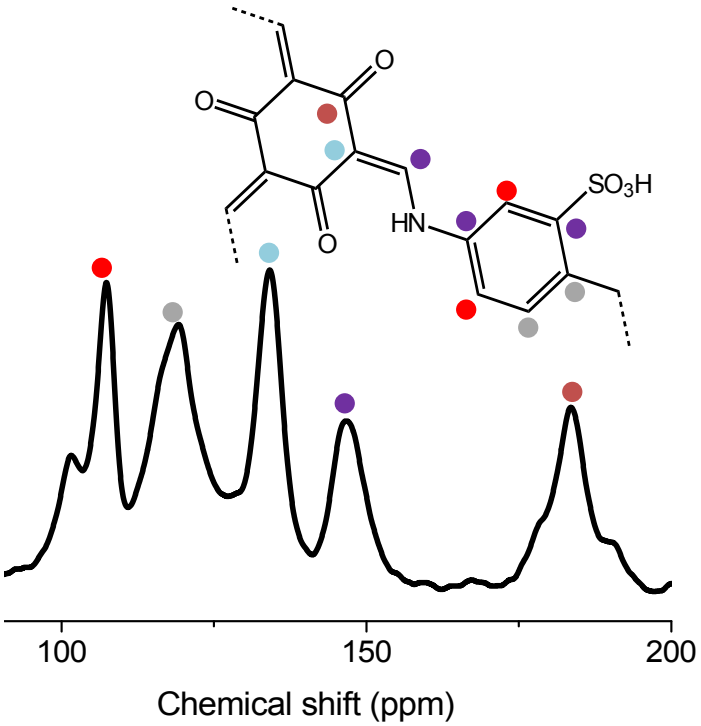

Figuer S14. Solid state ^{13}C NMR spectra of dpCOF-4.

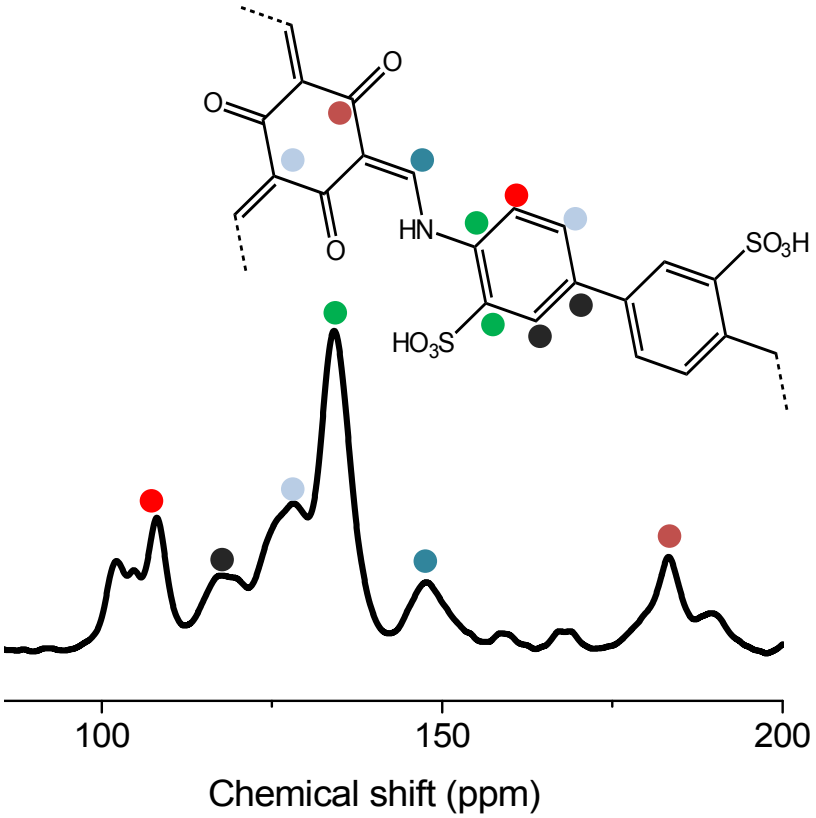

Figuer S15. Solid state ^{13}C NMR spectra of dpCOF-5.

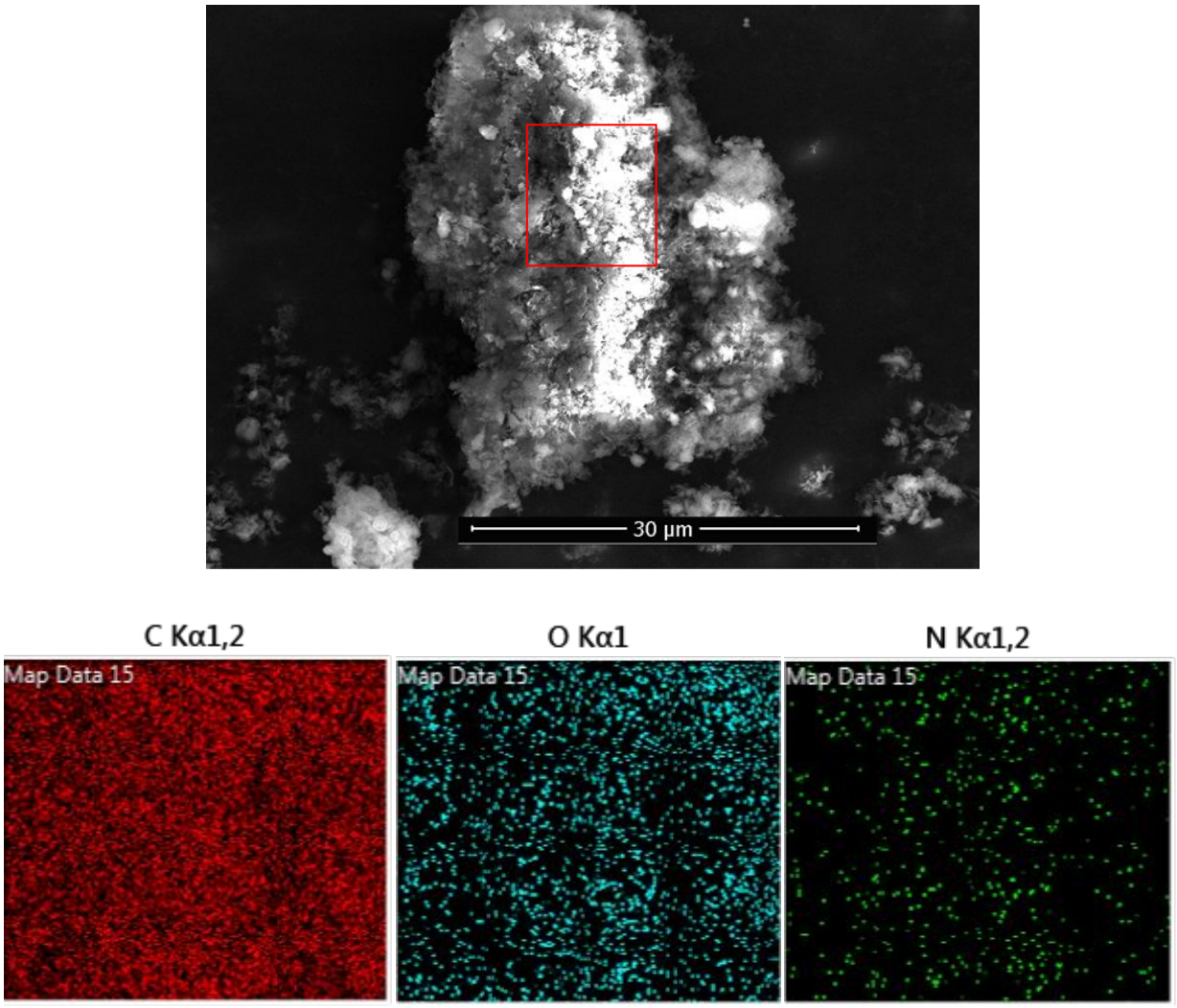

Figuer S16. The SEM image and EDS element mapping for dpCOF-2.

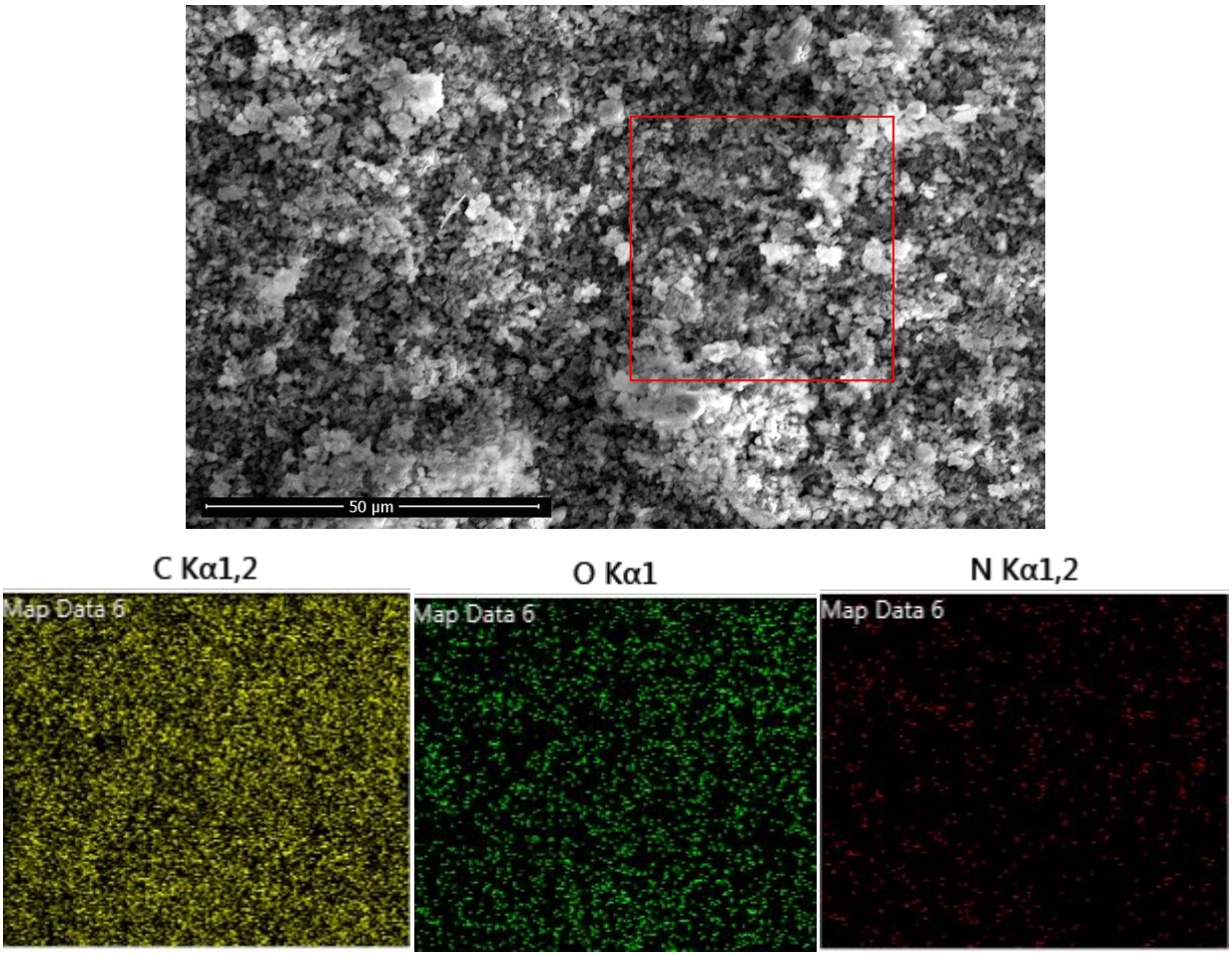

Figuer S17. The SEM image and EDS element mapping for dpCOF-3.

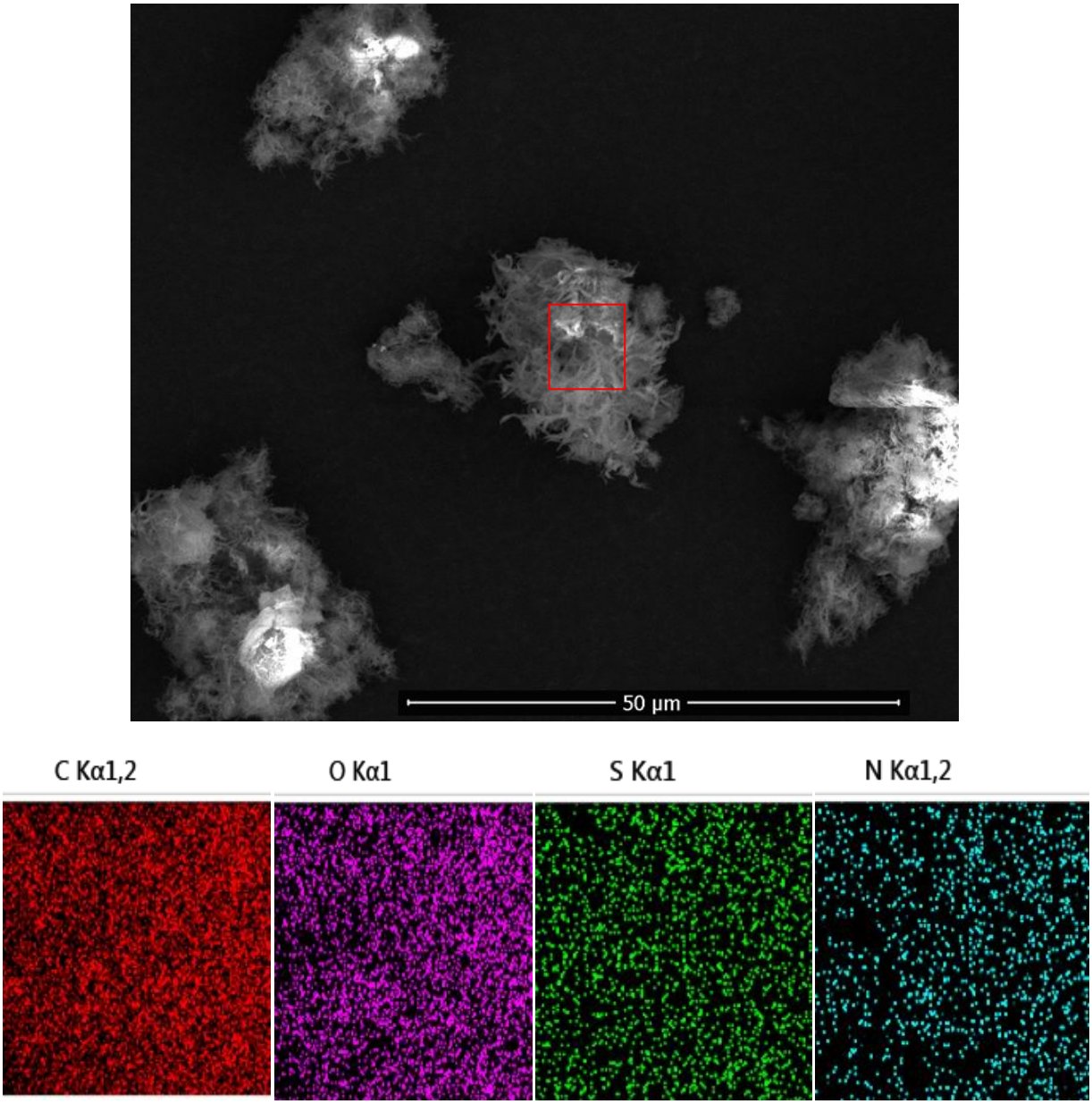

Figuer S18. The SEM image and EDS element mapping for dpCOF-4.

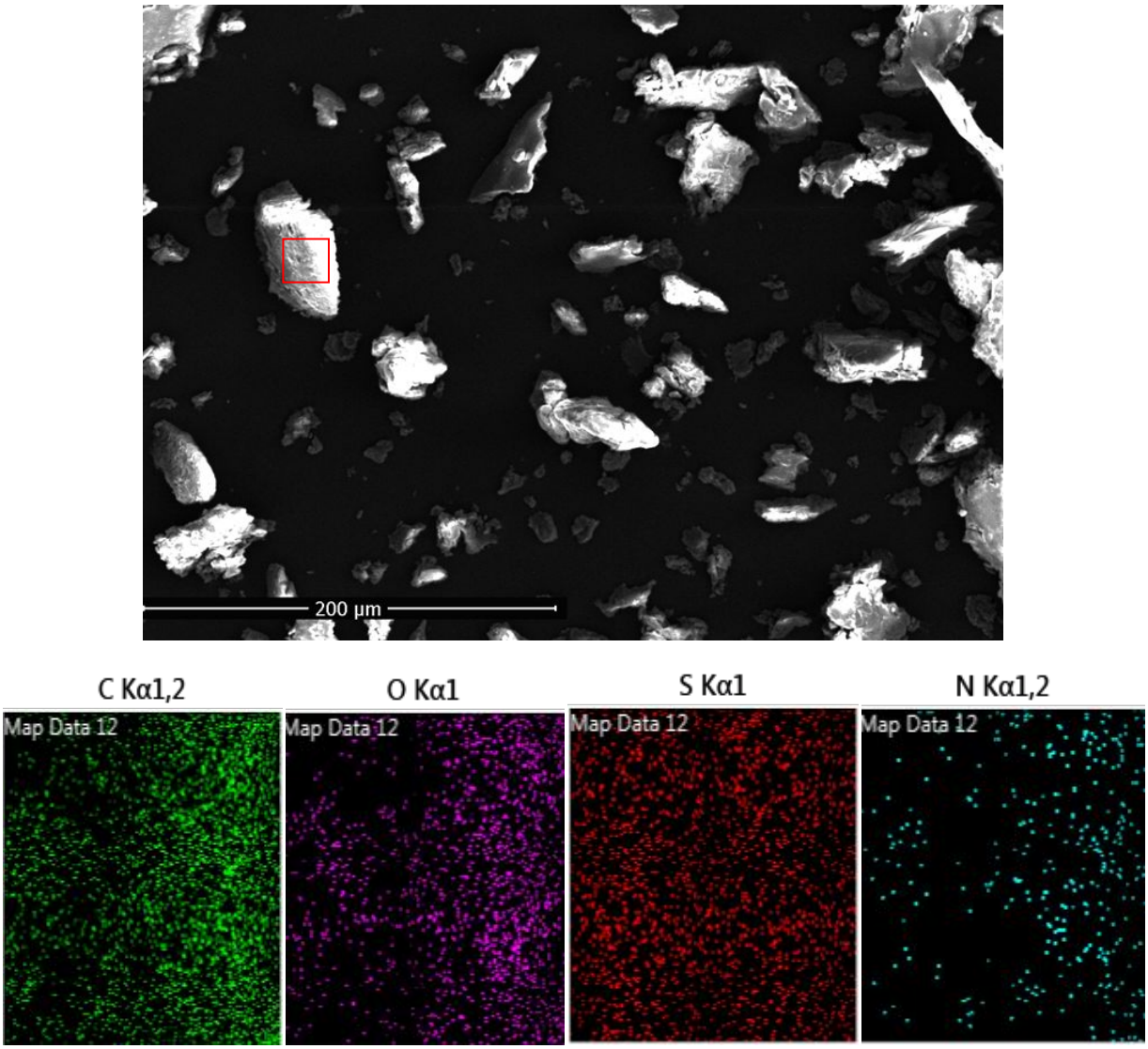

Figuer S19. The SEM image and EDS element mapping for dpCOF-5.

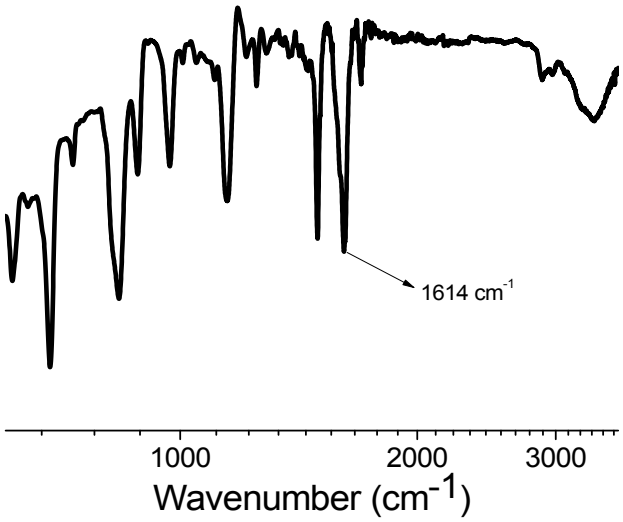

Figuer S20. The IR spectra of dpCOF-6.

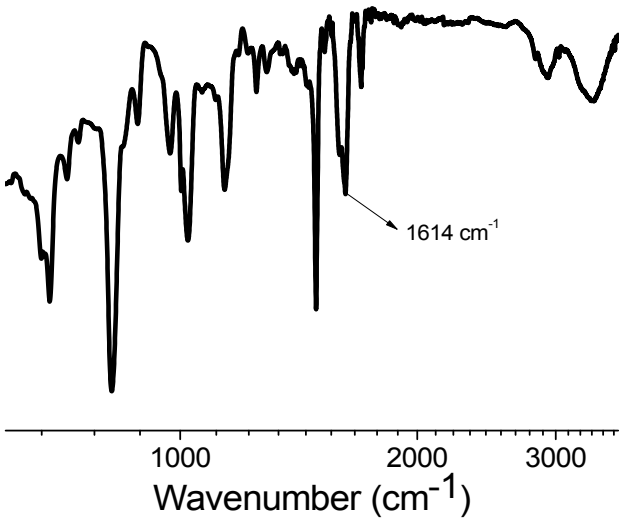

Figuer S21. The IR spectra of dpCOF-7.

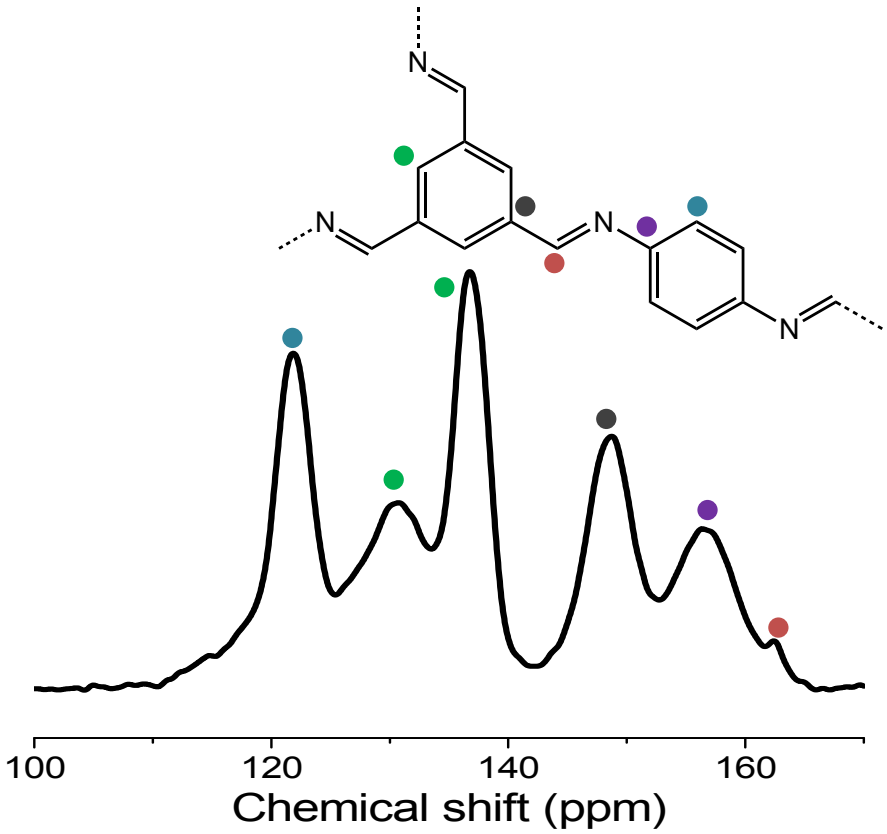

Figuer S22. Solid state ^{13}C NMR spectra of dpCOF-6.

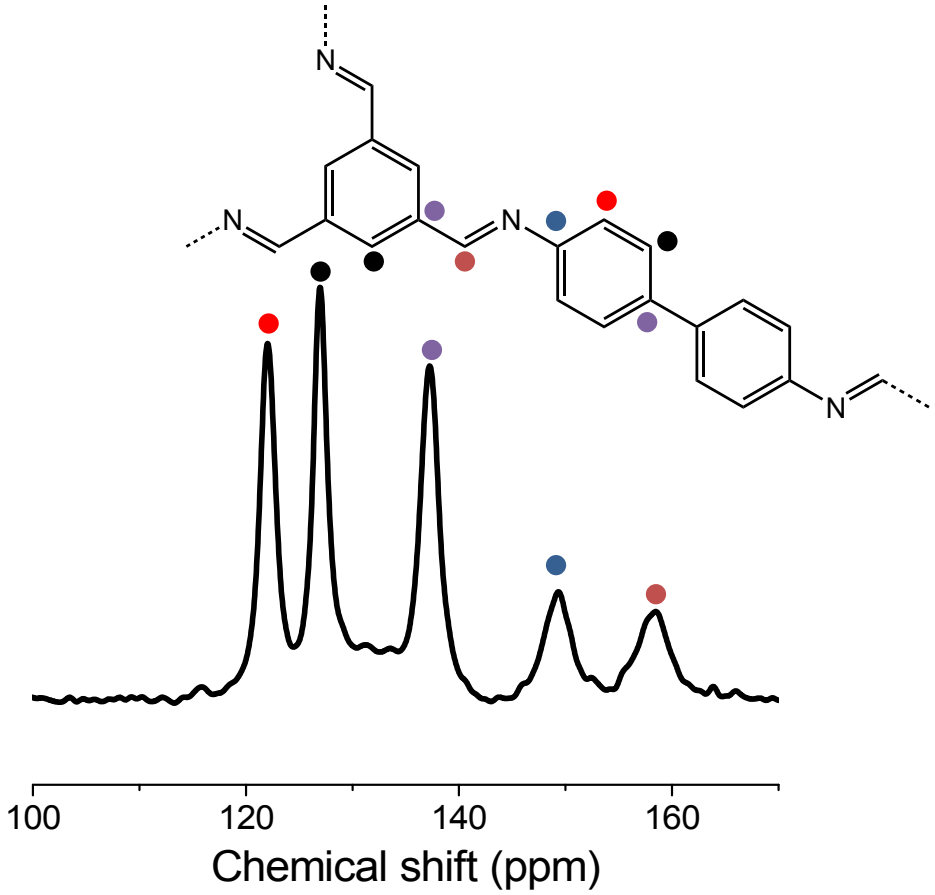

Figuer S23. Solid state ^{13}C NMR spectra of dpCOF-7.

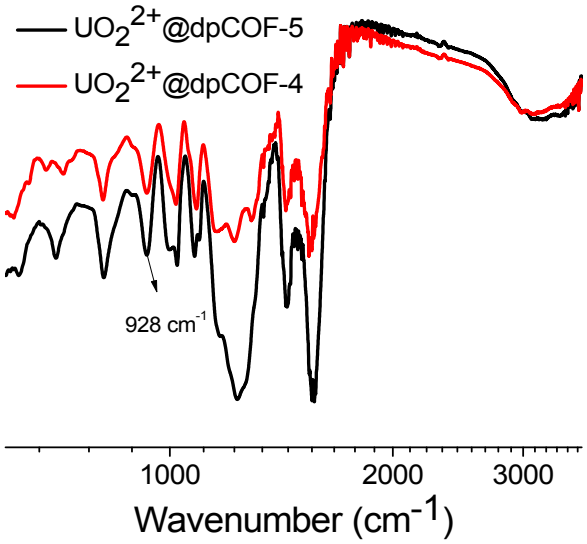

Figuer S24. The IR spectra of COF samples after UO_2^{2+} uptake.

Table S1. Fitting the adsorption data of dpCOF-5 and dpCOF-4 by Langmuir or Freundlich models.

Adsorbent	Langmuir model				Freundlich model		
	$q_{e,\,exp}$ (mg·g^{-1})	K_L (L·mg^{-1})	q_m (mg·g^{-1})	R^2	K_F (mg$^{1-1/n}$·g^{-1}·L$^{-1/n}$)	$1/n$	R^2
dpCOF-4	207	0.02390	226.244	0.9966	2.5234×10^4	0.3634	0.8613
dpCOF-5	416	0.01024	507.614	0.9952	2.2478×10^4	0.4915	0.9096